



OXFORD CENTRE FOR COLLABORATIVE APPLIED MATHEMATICS

# **Exploiting the Synergy Between Carboplatin and ABT-737 in the Treatment of Ovarian Carcinomas**

**by**

**Harsh Vardhan Jain  
Alan Richardson  
Michael Meyer-Hermann  
Helen M. Byrne**



# **Exploiting the Synergy Between Carboplatin and ABT-737 in the Treatment of Ovarian Carcinomas**

Harsh Vardhan Jain<sup>1</sup>, Alan Richardson<sup>2</sup>, Michael Meyer-Hermann<sup>3,4</sup>, Helen M. Byrne<sup>5,6</sup>

<sup>1</sup>Department of Mathematics, Florida State University, Tallahassee, Florida, USA.

<sup>2</sup>Institute for Science and Technology in Medicine, Keele University, Stoke-on-Trent, UK.

<sup>3</sup>Department of Systems Immunology, Helmholtz Centre for Infection Research, Braunschweig, Germany.

<sup>4</sup>Bio Centre for Life Science, Braunschweig University of Technology, Braunschweig, Germany.

<sup>5</sup>Oxford Centre for Collaborative and Applied Mathematics, Mathematical Institute, University of Oxford, Oxford, UK.

<sup>6</sup>Department of Computer Science, University of Oxford, Oxford, UK.

**Running Title:** Ovarian Cancer Treatment with Carboplatin and ABT-737

**Keywords:** ABT-737, Anti-Bcl-X<sub>L</sub> Therapy, Bcl-X<sub>L</sub>, Bax, Carboplatin, Mathematical Model, Ovarian Cancer

**<sup>7</sup>Funding Support**

**<sup>8</sup>Corresponding Author**

**Word Count:** Abstract 313 words; Body Text 5030 words (Introduction 740, Materials 1390, Results 1560, Discussion 1340); Quick Guide 810 words.

**Number of Figures and Tables:** 5 Figures, 0 Tables.

---

<sup>7</sup> HVJ: Support from NSF grant DMS 0931642. HMB: Support from Award No. KUK-C1-013-04 made by the King Abdullah University of Science and Technology (KAUST).

<sup>8</sup> Harsh Vardhan Jain, Department of Mathematics, Florida State University, 1017 Academic Way, Tallahassee, FL 32306 USA. Phone: +1 850 645 0523. Fax: +1 850 644 4053. Email: [jain@math.fsu.edu](mailto:jain@math.fsu.edu)

## Abstract

Platinum drug-resistance in ovarian cancers is a major factor contributing to chemotherapeutic resistance of recurrent disease. Members of the Bcl-2 family such as the anti-apoptotic protein Bcl-X<sub>L</sub> have been shown to play a role in this resistance. Consequently, concurrent inhibition of Bcl-X<sub>L</sub> in combination with standard chemotherapy may improve treatment outcomes for ovarian cancer patients. Here, we develop a mathematical model to investigate the potential of combination therapy with ABT-737, a small molecule inhibitor of Bcl-X<sub>L</sub>, and carboplatin, a platinum-based drug, on a simulated tumor xenograft. The model is calibrated against *in vivo* experimental data, wherein tumor xenografts were established in mice and treated with ABT-737 and carboplatin on a fixed periodic schedule, alone or in combination, and tumor sizes recorded regularly. We show that the validated model can be used to predict the minimum drug load that will achieve a predetermined level of tumor growth inhibition, thereby maximizing the synergy between the two drugs. Our simulations suggest that the time of infusion of each carboplatin dose is a critical parameter, with an 8-hour infusion of carboplatin administered each week combined with a daily bolus dose of ABT-737 predicted to minimize residual disease. We also investigate the potential of ABT-737 co-therapy with carboplatin to prevent or delay the onset of carboplatin-resistance under two scenarios. When resistance is acquired as a result of aberrant DNA-damage repair in cells treated with carboplatin, the model is used to identify drug delivery schedules that induce tumor remission with even low doses of combination therapy. When resistance is intrinsic, due to a pre-existing cohort of resistant cells, tumor remission is no longer feasible, but our model can be used to identify dosing strategies that extend disease-free survival periods. These results underscore the potential of our model to accelerate the development of novel therapeutics such as ABT-737, by predicting optimal treatment strategies when these drugs are given in combination with currently approved cancer medications.

**Major Findings:** The time of infusion of carboplatin doses is predicted to be a critical parameter that determines whether or not tumor remission is possible, when treating tumor xenografts periodically with a combination of carboplatin and ABT-737. Dosing strategies that prevent or delay the onset of carboplatin-resistance are identified when resistance is acquired, as a result of faulty DNA-damage repair following exposure to carboplatin, or is intrinsic, due to a pre-existing cohort of resistant cells.

## Quick Guide to Equations and Assumptions

A schematic of our model for the inhibition of ovarian cancer growth in response to carboplatin and ABT-737 application is shown in Figure 1A. A brief description of the model equations and the underlying assumptions follows (further details are included in the SI). The model comprises a system of time-delayed ordinary and partial differential equations that describe how  $N(t)$  and  $M(t, a)$ , the numbers of proliferating and arrested cancer cells (in millions) respectively, change over time, and how their evolution depends on  $C_T(t)$ ,  $A_C(t)$  and  $X(t)$ , the concentrations of tissue carboplatin (in  $\mu\text{M}$ ), intracellular ABT-737 (in nM) and intracellular free Bax (in nM), respectively. Here, time  $t$  is measured in days, and  $a$  is a time-like variable, representing the period of time a cell has spent in a growth-arrested state.

**Dynamics of proliferating cells.** Equation A models the growth of proliferating ovarian cancer cells ( $N$ ).

**Equation A:** 
$$\frac{dN}{dt} = \lambda_N N \left(1 - \frac{T}{K}\right) - \delta_N(X)N - \alpha_C(C_T)N + M(t, a = a_r)$$

Tumor cells are assumed to grow logistically in the absence of therapy, with growth rate  $\lambda_N$  and carrying capacity  $K$ . Arrested cells ( $M$ ) are assumed to compete for space with proliferating cells so that  $T(t)$  is the total (proliferating + arrested) number of cancer cells at time  $t$ . The rate of cell death  $\delta_N$  is assumed to depend on the intracellular concentration of free Bax ( $X$ ). Chemotherapy is applied periodically in the form of ABT-737 or carboplatin, alone or in combination. ABT-737 increases the rate of cell death, while carboplatin induces DNA damage and subsequent cell arrest at a rate  $\alpha_C$ , which depends on tissue carboplatin concentration  $C_T$ . The final term in Equation A represents the rate at which arrested cells recover and return to the proliferating pool.

**Dynamics of arrested cells.** Since cell death in response to carboplatin is not instantaneous, an age-structure is imposed on the arrested cells, age  $a$  representing the amount time for which a cell has been arrested. Following the general McKendrick equation for age-structured populations [25], the dynamics of arrested cells are assumed to be governed by the following hyperbolic partial differential equation:

**Equation B:** 
$$\frac{\partial M}{\partial t} + \frac{\partial M}{\partial a} = -\delta_M(C_T(t-a), X(t), a)M$$

Arrested cells undergo apoptosis at a rate  $\delta_M$  proportional to the tissue concentration of carboplatin present at the time of cell arrest ( $C_T(t-a)$ ), and the intracellular concentration of free Bax ( $X$ ). Equation B is solved subject to the boundary condition:

$$M(t, 0) = \alpha_c(C_T)N$$

Based on experimental observations in [13], arrested cells are assumed to start undergoing apoptosis 12-16 hours after the application of carboplatin, and cells that have not undergone apoptosis after a characteristic time  $a_r = 48$  hours are assumed to recover and return to the proliferating population, this return being instantaneous so that  $M(t, a) = 0$  for  $a > a_r$ .

Additionally, the number of arrested cells at time  $t$  is given by  $\int_{t-a_r}^t M(t, a)da$ .

**Carboplatin pharmacokinetics and pharmacodynamics.** Carboplatin is administered intraperitoneally, either as a series of periodic boli or via continuous infusion. Its pharmacokinetics are assumed to be governed by a 3-compartment model: the peritoneal cavity comprising the first compartment, the circulatory system and well-vascularized tissue comprising the second, and tissues and organs with poor vascular perfusion comprising the third compartment. Since tumor vasculature is highly disorganized and of a poor functional quality [29], we assume that the tumor resides in the peripheral compartment. Thus, proliferating

cells are assumed to undergo cell cycle arrest in response to drug-induced DNA damage at a rate  $\alpha_C$ , taken to be an increasing and saturating function of peripheral tissue carboplatin concentration ( $C_T$ ).

**ABT-737 pharmacokinetics and pharmacodynamics.** ABT-737 is administered intraperitoneally as a bolus injection, on a fixed periodic schedule, and the following 3-compartment model is assumed to govern its pharmacokinetics. The first compartment is the peritoneal cavity into which the drug is injected. From here, ABT-737 enters the systemic circulation, taken as the second compartment, via vasculature in the peritoneum, and is finally taken up by cells into the third, intracellular compartment where it interacts with the intracellular regulators of apoptosis, the Bcl-2 family of proteins (see Figure 1B).

For simplicity, the pro- and anti-apoptotic members of the Bcl-2 family are each represented by a single candidate protein: Bax ( $X$ ) represents the pro-apoptotic proteins and Bcl-X<sub>L</sub> ( $B$ ) the anti-apoptotic ones. The interactions between these proteins and intracellular ABT-737 ( $A_C$ ) are shown in Figure 1B. Given that members of the Bax-like subfamily control the release of cytochrome c from the mitochondria, which results in eventual caspase activation and cell death [7], the rates at which proliferating and arrested cells undergo apoptosis ( $\delta_N$  and  $\delta_M$ , respectively) are assumed to be increasing functions of free intracellular Bax,  $X$ .

**The emergence of carboplatin-resistance:** When considering the emergence of resistance to carboplatin, the proliferating cell population is subdivided into two classes – carboplatin-sensitive and carboplatin-resistant, or insensitive. Following [13] where ovarian cancer cell lines with different sensitivities to carboplatin were observed to be comparably responsive to ABT-737, both carboplatin-sensitive and resistant cells are assumed to be equally sensitive to ABT-737.



## Introduction

Although ovarian cancer accounts for only 3% of cancers in women, it is the fifth most common cause of cancer death in women in the developed world [1]. Primary treatment for advanced ovarian cancer consists of cytoreductive surgery followed by adjuvant chemotherapy. The chemotherapeutic regimen typically combines a taxane such as paclitaxel with a platinum-based drug such as carboplatin, which causes cell death by inducing DNA damage. While patients initially respond well to therapy, most ultimately relapse, with recurrent disease being associated with progressive resistance to platinum-based therapy [2, 3]. Consequently, 5-year survival rates for women with advanced ovarian cancer are less than 25% [4].

Several factors may contribute to platinum drug-resistance (for a comprehensive review, see [5,6]). We are concerned with resistance arising as a result of increased expression of the anti-apoptotic protein Bcl-X<sub>L</sub>. Bcl-X<sub>L</sub> belongs to the Bcl-2 family of intracellular proteins that regulates programmed cell death, or apoptosis [7]. Previous studies have revealed a significant correlation between Bcl-X<sub>L</sub> expression and carboplatin-resistance [8-10], and increased sensitivity to standard chemotherapeutic agents of ovarian cancer cell lines when Bcl-X<sub>L</sub> expression is inhibited [11-13]. Therefore, concomitant inhibition of Bcl-X<sub>L</sub> in combination with adjuvant chemotherapy may improve treatment outcomes for ovarian cancer patients.

In [13], Witham et al. assess the therapeutic potential of treating an ovarian cancer cell line that expresses Bcl-X<sub>L</sub> with carboplatin and ABT-737, a small-molecule inhibitor of Bcl-X<sub>L</sub>. Results from *in vitro* cell proliferation assays revealed greater inhibition of cell-growth and more rapid apoptosis when carboplatin was combined with ABT-737, than when it was administered as a single agent. Further, the times at which the two drugs are administered were also shown to be an important determinant of therapy efficacy, with an ABT-737 dose immediately following carboplatin found to yield the greatest extent of cell death. To understand better these

experimental findings, we have previously developed a biochemically-motivated model for the growth of *in vitro* ovarian cancer [14], that was validated against available experimental data. A key prediction of our model is that the experimentally observed synergy between ABT-737 and carboplatin is due to the reduced ability of DNA-damaged cells to tolerate changes in intracellular Bcl-X<sub>L</sub> levels.

Here, we develop a mathematical model of ovarian cancer xenograft growth to test the efficacy of combining ABT-737 and carboplatin for the treatment of ovarian cancers growing *in vivo*. While several models of cancer therapy involving platinum-based compounds [15,16] or drugs targeting the Bcl-2 family [17,18] have been proposed, to the best of our knowledge this is the first attempt to model the effect of a combination of these drugs on tumor growth. Since the active processing of administered drugs by the body may have a significant effect on their efficacy and how they interact, we need to incorporate the pharmacokinetics of carboplatin and ABT-737 in our model. We parameterize our model using experimental data reported in [13], wherein monoclonal ovarian tumor xenografts established in mice were treated with fixed doses of carboplatin and ABT-737 administered periodically and time-courses of tumor growth inhibition recorded. The validated model is then used to identify dosing strategies for the treatment of monoclonal tumors, which either lead to fastest times to minimal residual disease or minimize total drug load to achieve a predetermined level of tumor growth inhibition. The infusion time of carboplatin doses is predicted to be an important determinant of the long-term response of tumors to therapy, this testable prediction underscoring the practical significance of our results.

As mentioned earlier, a major cause of long-term treatment failure in ovarian cancer patients is the emergence of carboplatin-resistance. Given its synergistic action with carboplatin, ABT-737 co-therapy has the potential to prevent or delay treatment failure. We investigate this potential in the case when resistance to carboplatin is driven by genetic or epigenetic aberrations. Such

aberrations arise in two different ways. In *acquired resistance*, genetic mutations emerge after the administration of chemotherapy, as a result of faulty DNA repair in cells treated with carboplatin. Alternatively, in *intrinsic resistance*, epigenetic changes and/or mutations in cellular DNA are induced by factors that include damage from environmental agents, oxidative damage from the byproducts of cellular metabolism, or aberrant DNA replication as a cell prepares for division. Therefore, a small population of resistant cells may already be present before the administration of chemotherapy. By distinguishing between these alternative scenarios of drug resistance, our model represents a useful tool with which to design individualized treatment protocols targeted against carboplatin-resistance.

## Material and Methods

### Model Foundation

Our model of ovarian cancer xenograft growth and its response to carboplatin and ABT-737 therapy can be described in mathematical terms by a coupled system of ordinary and partial differential equations (further details are included in the SI), which govern the temporal dynamics of the following key variables: the numbers in millions of proliferating ( $N$ ) and arrested ( $M$ ) cancer cells, the concentration in  $\mu\text{M}$  of intraperitoneal ( $C_{\text{perit}}$ ), plasma ( $C_P$ ) and tissue ( $C_T$ ) carboplatin, the concentration in  $\text{nM}$  of intraperitoneal ( $A_{\text{perit}}$ ), plasma ( $A_P$ ) and intracellular ( $A_C$ ) ABT-737, and the intracellular concentrations in  $\text{nM}$  of Bcl- $X_L$  ( $B$ ), Bax ( $X$ ), Bcl- $X_L$ -Bax complex ( $Q$ ) and Bcl- $X_L$ -ABT-737 complex ( $P$ ). A schematic detailing the response of the cancer cells to therapy is shown in Figure 1A. In the sections that follow, the principles underlying our model formulation are introduced.

## **Tumor Xenograft Growth and Regulation of Cellular Apoptosis**

The growth rate of untreated tumor xenografts is typically exponential at early times, and plateaus as they become larger [19]. Consequently, we assume that ovarian cancer cells grow logistically in the absence of treatment. We remark that models of periodic chemotherapy based on the logistic equation have been proposed previously [20- 23]. The basic proliferation rate  $\lambda_N$  of cancer cells and the carrying capacity  $K$  of their microenvironment are chosen by fitting time-courses of cell numbers to data from untreated tumor xenografts in [13], as shown in Figure 1C (black curve).

We account for the regulation of cell death by the Bcl-2 family of proteins in the following way. For simplicity, and in the absence of appropriate experimental data, we represent each of the pro- and anti-apoptotic sub-families of the Bcl-2 family by a single variable. Given the specificity of ABT-737 for Bcl-2 and Bcl-X<sub>L</sub>, and its similar binding affinity for both these molecules [24], we represent the anti-apoptotic members of the Bcl-2 family by Bcl-X<sub>L</sub>. Further, Bax is taken to represent the pro-apoptotic proteins since it is the members of the Bax-like subfamily which controls the release of cytochrome c from the mitochondria that leads to caspase activation, that is followed by cell death [7]. The rate of cell death is consequently assumed to be an increasing function of free intracellular Bax.

We now describe the effect on the growing tumor of the application of carboplatin and ABT-737.

### **Effect of ABT-737 on Proliferating Cells**

Upon application, ABT-737 enters the proliferating tumor cells where it binds to, and sequesters Bcl-X<sub>L</sub> (see Figure 1B), causing levels of free Bax to rise, thereby increasing the rate of cell death. Parameters relating to the death rate  $\delta_N$  of proliferating cells are chosen by fitting time-courses of estimated cell numbers to tumor xenograft growth inhibition data taken from [13],

wherein IGROV-1 xenografts established in mice were treated daily with a fixed dose of ABT-737 administered intraperitoneally for 4 weeks. The best fit is shown in Figure 1C (red curve).

### **Effect of Carboplatin on Proliferating Cells**

The cytotoxicity of carboplatin is primarily due to damage induced by the formation of intrastrand adducts at the nucleophilic N7 sites in the DNA. This damage stimulates the activation of downstream pathways that lead to cell cycle arrest, followed by either survival if the DNA damage is repairable, or apoptosis [6]. Consequently, upon drug application, proliferating cells are assumed to undergo cell cycle arrest at a rate that is assumed to be an increasing and saturating function of the tissue carboplatin concentration,  $C_T$ , so that as the drug dose (and correspondingly the level of DNA damage) increases, the rate of cell cycle arrest also increases up to a maximum level.

### **An Age-structured Model of Arrested Cell Dynamics**

The arrested cells are removed to a separate compartment, where they either undergo apoptosis or recover and return to the proliferating population. In [13], apoptosis was routinely observed in cells 16 hours post carboplatin administration. Consequently, arrested cell dynamics are described by applying the general McKendrick equation that is widely used to model age-structured populations [25] (a schematic is shown in Figure 1A), where the rate of arrested cell death is taken to be a function of the time for which the cells have been arrested. Cell cytotoxicity has been found to correlate linearly with the amount of platinum bound to the DNA, and hence the extent of DNA damage [6]. Accordingly, the rate of arrested cell death is taken to be linearly proportional to the amount of tissue carboplatin at the time of cell-cycle arrest. Finally, the length of time for which a cell can remain in an arrested state is limited. We therefore assume that cells that have not undergone apoptosis after a characteristic time (taken to be 48 hours) recover and return to the proliferating population.

## Tumor Cell Response to Combination Therapy

As in the case of proliferating cells, when ABT-737 is co-administered with carboplatin, it is taken up by the arrested cells where it binds to, and sequesters Bcl-X<sub>L</sub> (see Figure 1B), causing levels of free Bax to rise. Further, in [14] the observed synergy between carboplatin and ABT-737 was shown to be due to an increased dependence of DNA-damaged cells on Bcl-X<sub>L</sub> for survival. Accordingly, the rate of arrested cell death is taken also to be proportional (with constant of proportionality  $\rho_s$ ) to free intracellular Bax.  $\rho_s$  is an important parameter in our model: it represents the sensitivity of the arrested cells to changes in Bax, and hence provides a quantitative measure of the degree of synergy between carboplatin and ABT-737.

Parameters relating to the rate at which proliferating cells become growth arrested  $\alpha_C$  and the rate at which arrested cells die  $\delta_M$  are chosen by fitting time-courses of estimated numbers of cells to tumor xenograft growth inhibition data taken from [13], wherein IGROV-1 xenografts established in mice were treated weekly with a fixed dose of carboplatin administered intravenously for 4 weeks as a single agent, or in combination with a fixed daily dose of ABT-737. The best fits are shown in Figure 1D.

The functional forms used in our model for the response of proliferating and arrested cells to carboplatin and ABT-737 account for their pharmacokinetics, which are described below.

### Carboplatin Pharmacokinetics

Carboplatin was administered intraperitoneally in [13] and its pharmacokinetics are assumed to be governed by the following 3-compartment model. Experimental evidence suggests that small molecular weight drugs (molecular weight of carboplatin = 371.2 Da [26]) delivered intraperitoneally are readily absorbed through the peritoneal vasculature to enter systemic circulation [27, 28]. Consequently, the peritoneal cavity is taken to be the first compartment.

Since the time-activity curve of carboplatin in the blood plasma of mice has been shown to be biphasic [26], the circulatory system together with highly vascularized and well-perfused organs are taken to be the second or central compartment, and the peripheral organs and tissues with relatively poor vascular perfusion account for the third compartment. As tumor vasculature is characterized by its poor functional quality, and is highly disorganized [29], we assume that the tumor resides in the peripheral pharmacokinetic compartment of carboplatin. The equations governing carboplatin pharmacokinetics are given in section S3 of the SI.

We investigate the effect on tumor response of administering the same dose of carboplatin as either a rapid infusion or bolus, or a continuous infusion lasting several hours, when given in combination with ABT-737. In fact, the time of infusion ( $T_i$ ) of each dose of carboplatin is predicted to be a critical parameter in determining the therapeutic efficacy of combination therapy.

### **ABT-737 Pharmacokinetics**

ABT-737 is administered intraperitoneally in [13] and its pharmacokinetics are assumed to be governed by the following 3-compartment model. Since ABT-737 is a low molecular weight drug (molecular weight = 813.4 Da [24]), as in the case of carboplatin, the peritoneal cavity is taken as the first compartment, and the systemic circulation as the central (and second) compartment. In our model, we explicitly account for the regulation of cell death by the Bcl-2 family of proteins. Therefore, a third intracellular compartment, into which the drug permeates from the systemic circulation, is included. The equations governing ABT-737 pharmacokinetics are given in section S2 of the SI.

Details of parameter estimation described in this section, and a list of parameter values can be found in the SI.

## Results

Having calibrated our model against *in vivo* experimental data (Figure 1), a series of numerical experiments are carried out to identify dosing strategies that exploit the synergy between carboplatin and ABT-737. Since our model formulation is based on experiments that studied the response of monoclonal xenografts to therapy, we start by considering a tumor that comprises a homogenous population of carboplatin-sensitive cells. A major aim of our model is to investigate the potential of co-treatment with ABT-737 to prevent or delay the onset of carboplatin-resistance that is a leading cause of treatment failure. We therefore also simulate the treatment of a tumor that consists of carboplatin-sensitive and -resistant cells. The emergence of resistance under two distinct scenarios is considered: (i) acquired resistance resulting from faulty DNA damage repair; and (ii) intrinsic resistance resulting from a pre-existing cohort of resistant cells.

Following [13], in all simulations carboplatin is assumed to be administered on a weekly schedule and ABT-737 on a daily schedule. When simulating monoclonal xenograft treatment, the initial number of tumor cells is calculated from the size of tumors at the initiation of therapy. As can be seen from the cell number time-courses in Figure 1D, the weekly administration of carboplatin induces oscillations in tumor size. Therefore, cell numbers averaged over the period of carboplatin administration (7 days) are used to make quantitative comparisons between tumor responses to various treatment strategies (see Figures 2-5). Tumors are assumed to have achieved a steady-state average size if the relative change in average tumor cell numbers between successive weeks is less than 0.001% and time to minimal residual disease ( $T_m$ ) is defined as the period for which therapy must be administered so that the average number of



cells is less than 1. All model simulations are carried out in Matlab, a technical computing language, the numerical methods being described in Section S4 of the SI.

### **Optimal Relative Doses for Monoclonal Tumors**

We consider the following optimization problem in the treatment of cancers with a combination of two or more drugs – “What drug doses achieve a predetermined level of cell kill while minimizing patient drug load?”

For illustrative purposes, we use our model to predict the optimal doses of carboplatin and ABT-737 required to achieve a 67% growth inhibition in monoclonal tumors at the end of 4 weeks of therapy (that is, the treatment time reported in [13]). Note that minimizing the drug load is equivalent to minimizing the Combination Index (CI) of the two drugs, defined as  $CI_{67} = (C/C_{67}) + (A/A_{67})$  [30], subject to the constraint that 4 weeks post-therapy, tumor size is 33% of its untreated value. Here,  $C_{67}$  and  $A_{67}$  are the amounts of drugs required to achieve a 67% growth inhibition when administered as single-agents,  $C$  is the weekly bolus dose of carboplatin and  $A$  is the daily bolus dose of ABT-737 when these drugs are used in combination.  $C$  is varied between 0 and  $C_{67}$ , and the constraint used to generate values of  $A$ . This represents an optimization problem for the function  $CI_{67}$  in a single variable  $C$  that assumes values on a closed and bounded interval and, hence,  $CI_{67}$  attains its minimum therein.

A phase diagram of the drug doses required to inhibit tumor growth by 67% after 4 weeks is shown in Figure 2A, with ABT-737 doses plotted along the abscissa and carboplatin doses plotted along the ordinate.  $CI_{67}$  values for various dose combinations are enumerated along the curve. A weekly bolus of 17.8 mg/kg carboplatin combined with a daily bolus dose of 86.5 mg/kg ABT-737 is predicted to minimize the  $CI_{67}$  (dashed lines). We remark that similar curves can be computed for other levels of tumor growth inhibition at the end of a fixed time period, and for other treatment strategies. The tumor cell time-course data corresponding to these optimal

doses presented in Figure 2B reveal that the levels of tumor growth inhibition after 4 weeks of treatment with either 86.5 mg/kg ABT-737 administered as a single agent or 17.8 mg/kg carboplatin administered weekly as a single agent are 31.4% and 28.9% respectively. The predicted level of growth inhibition when these doses are combined is 67%.

Simulating treatment for periods longer than 4 weeks with drug doses fixed at the above values further underscores the synergy between the two drugs. Figure 2C shows that if the tumor is allowed to reach its (average) steady state size, the levels of tumor growth inhibition decrease to 31.7% and 23.1% when ABT-737 or carboplatin are applied as monotherapy, respectively, whereas combination treatment results in a 79.2% tumor growth inhibition in the long term.

### **Optimal Dose Scheduling for Monoclonal Tumors**

We next use our model to identify an optimal dose-delivery strategy when monoclonal tumors are treated with a combination of ABT-737 and carboplatin for long times. Following the experimental protocol in [13], the doses of carboplatin and ABT-737 are fixed at 30 mg/kg and 100 mg/kg, respectively. In particular, the dependence of tumor response on two key parameters, the carboplatin infusion time  $T_i$ , and the sensitivity  $\rho_s$  of arrested cells to changes in intracellular Bax, is investigated.

With  $\rho_s$  fixed at its baseline value ( $\rho_s = 135$ ), steady-state values of average cell number are calculated as  $T_i$  varies between 0 hours (bolus dose) and 120 hours. Figure 3A reveals that minimal survival of tumor cells is predicted for  $1 \leq T_i \leq 25$ . If  $T_i < 1$  hour, even though significant levels of long-term tumor growth inhibition can be achieved (see inset), complete remission is not possible. Additionally, for  $T_i > 25$  hours, the level of growth inhibition decreases rapidly as  $T_i$  increases. In Figure 3B, we show how  $T_m$ , the length of time for which treatment must be administered in order to achieve minimal survival of tumor cells varies when  $1 \leq T_i \leq 25$ . As  $T_i$

increases from  $T_i = 1$ ,  $T_m$  decreases, attaining a minimum of 215 days when carboplatin is administered via weekly infusions lasting 8 hours, and then increases for larger values of  $T_i$ .

$T_m$  depends not only on the carboplatin infusion time  $T_i$ , but also on  $\rho_s$ , the sensitivity of arrested cells to changes in intracellular Bax. For each value of  $\rho_s$  between 0 and 600, the minimum of  $T_m$  is calculated as  $T_i$  is varied between 0 and 120 hours. Figure 3C shows that this minimum decreases rapidly as  $\rho_s$  increases from  $\rho_s = 0$ , plateauing at a value of 215 days for large values of  $\rho_s$ . In all considered cases,  $T_m$  attains its minimum for  $T_i = 8$  hours (data not shown).

### **Emergence of Acquired Resistance**

We now investigate the potential of ABT-737 co-therapy to prevent or delay the emergence of carboplatin-resistance. Since ovarian cancers are frequently diagnosed at a late stage [31], we simulate the application of therapy to tumors that have already attained their maximal untreated size (carrying capacity). As several carboplatin-sensitive and resistant ovarian cancer cell lines have been shown to have similar sensitivity to ABT-737 [13], carboplatin-sensitive and -resistant tumor cells are assumed to be equally sensitive to ABT-737 in our model.

We first assume that there is a small probability that cells recovering from a carboplatin-induced state of arrest experience aberrant DNA damage repair, resulting in a resistant phenotype. We assume further that no resistant cells exist at the start of treatment. Figure 4A-D shows predicted average cell number time-courses for a tumor treated with increasing weekly bolus doses of carboplatin only. A weekly dose of 1300 mg/kg is required to affect a cure and prevent the emergence of resistance (Figure 4D). Smaller doses result in transient decreases in tumor size, with the tumor eventually recovering to its untreated size (Figure 4A-C) due to the dominance of resistant cells. In contrast, Figure 4E reveals that a weekly bolus dose of 30 mg/kg carboplatin combined with a daily dose of 100 mg/kg ABT-737 may prevent the onset of carboplatin-resistance and result in tumor-growth control at 6.5% of its untreated level at steady-

states. Significantly, the same combination, with carboplatin administered as an 8-hour infusion instead of as a bolus, is predicted to result in tumor remission within 150 days of treatment (Figure 4F).

### **Treatment of Tumors with Intrinsic Resistance**

Finally, we consider the response of a tumor which contains a small population of carboplatin-resistant cells at the start of treatment. Figure 5A-C shows predicted average cell number time-courses when the tumor is treated with increasing weekly bolus doses of carboplatin alone. Now, even doses in excess of 1300 mg/kg (Figure 5C) are unable to induce sustained tumor regression. Further, in contrast to the case of acquired resistance, a weekly bolus dose of 30 mg/kg carboplatin combined with a daily dose of 100 mg/kg ABT-737 is unable to prevent the onset of carboplatin-resistance (Figure 5D), with the tumor recovering to 65.2% of its untreated size after a transient decline in cell numbers. Figure 5E shows that, administering carboplatin as an 8-hour infusion results in the tumor reaching a much lower minimum at around day 150 of treatment, indicating a possible period of disease-free survival, defined as clinically undetectable disease. However, resistant cells eventually dominate and the tumor escapes from therapy-induced growth control. Increasing the daily ABT-737 dosage to 500 mg/kg in combination with 30 mg/kg carboplatin given as a 8-hour infusion is predicted to increase the disease-free survival time, and lead to a greater level of long-term growth control (Figure 5F).

### **Discussion**

The development of carboplatin-resistance is a major factor hampering the successful treatment of ovarian cancer with standard chemotherapy (carboplatin + paclitaxel). This resistance may be mediated in part by members of the Bcl-2 family that regulate cellular apoptosis. Consequently,

it has recently been proposed [13] that inhibiting anti-apoptotic proteins such as Bcl-X<sub>L</sub> may improve the efficacy of carboplatin. A critical challenge in the development of such novel therapeutics is to arrive at treatment strategies that maximally exploit any synergy between the drugs, and to identify patients who might benefit from such a combination.

In this article, we have presented a mathematical model of the growth of an ovarian cancer xenograft and its treatment with carboplatin, and ABT-737, a small molecule inhibitor of Bcl-X<sub>L</sub>. The main goal of this research was to identify protocols for the treatment of ovarian cancer *in vivo* that exploit the molecular basis of synergy between the two drugs. To this end, we explicitly incorporated the intracellular regulation of apoptosis by the Bcl-2 family of proteins, and introduced a cell-age structured model to simulate the effect of carboplatin on cell fate. Further, to reflect the *in vivo* setting, detailed pharmacokinetics of carboplatin and ABT-737 were also included. The model was validated by fitting time-courses of ovarian cancer xenograft growth inhibition reported in [13]. The good agreement between model simulations and experimental data give confidence that the model is able accurately to describe the underlying biology.

We first simulated the treatment of tumors that consist of a monoclonal population of cells. Doses of carboplatin and ABT-737 required for a certain level of tumor growth inhibition were calculated, which minimize patient drug load and hence maximize the synergy between the two drugs. The method we describe here can in principle be applied to any drug combination and can easily be tailored to account for side effects of the drugs under evaluation, once appropriate data is available to support the model. Using our approach, physicians can estimate the impact of different doses of drugs in combination on the therapeutic response of patients. As combination therapies are increasingly being applied in oncology, models such as the one we present here can lead to significant time and cost savings by minimizing the choices that need to be examined experimentally. Further, such modeling can also be used to arrive at optimal

individualized treatment strategies for evaluating combinations of chemotherapeutic drugs in clinical trials.

An equally important application of the model is predicting the long-term response to therapy. An exhaustive search of parameter space revealed a control parameter that is predicted to be a critical determinant of tumor growth dynamics when at least 1 year of carboplatin and ABT-737 co-therapy is simulated. This is the infusion time of the weekly dose of carboplatin. Carboplatin is typically administered as an infusion lasting 15 minutes or more when given in combination with paclitaxel. In fact, it has been proposed that the efficacy of carboplatin is directly linked to its AUC (Area Under the Curve) value, and the Calvert formula currently used to determine its clinical doses makes use of this fact [32]. However, our model simulations suggest that when combined with ABT-737, the efficacy of combination therapy is determined not only by the AUC of carboplatin, but also by the duration of drug infusion. Our simulations predict that weekly carboplatin infusions lasting between 1 and 25 hours combined with daily doses of ABT-737 result in the minimal survival of tumor cells. This is because, when administered as a rapid infusion, the peak tissue concentration of carboplatin is high, and a high level of DNA damage is induced in cancer cells from which they are unlikely to recover, irrespective of changes in intracellular Bcl-X<sub>L</sub> levels. Consequently, the synergy between the carboplatin and ABT-737 is muted. Equally, slower infusions of carboplatin result in extremely low tissue concentrations of the drug, so that the level of DNA damage induced in cells is minimal, and even with inhibited Bcl-X<sub>L</sub> levels, arrested cells are likely to recover to the proliferating pool. Note that since ABT-737 is administered daily and has a slow clearance rate, its intracellular concentration rapidly achieves a non-zero mean (see Figure S2D in SI). Therefore, changing the infusion time of ABT-737 administration is not predicted to alter our predictions.

Further, numerical simulations were carried out to identify the carboplatin infusion time that results in the fastest time to minimal residual disease. These times were observed to decrease

rapidly to a minimum value as the sensitivity of arrested cells to intracellular Bax concentration ( $\rho_s$ ) was increased. The parameter  $\rho_s$  is a quantitative measure of the synergy between the carboplatin and ABT-737 and can be important in identifying a subclass of patients who would most benefit from such a combination of drugs. However,  $\rho_s$  cannot be directly measured from experiments. As demonstrated here, we can infer its value by fitting model simulations to tumor xenograft growth inhibition data when both drugs are given in combination.

ABT-737 co-therapy is now being developed to improve the efficacy of carboplatin, and may aid in delaying the onset of chemoresistance in ovarian cancers. We therefore investigated the therapeutic potential of combinations of ABT-737 and carboplatin to treat ovarian cancers in which carboplatin-resistance arises in two distinct scenarios. Genetic mutations leading to resistance may be acquired as a result of faulty DNA damage repair when cells try to recover from carboplatin administration. Carboplatin-resistance may also be an intrinsic property of the cancer, stemming from resistant cells present when treatment starts. A key strength of our approach is the ability to distinguish between these scenarios. For instance, in the case of acquired resistance, model simulations predicted that preventing cells that have undergone carboplatin-induced DNA-damage from recovering and returning to the proliferating population precludes the emergence of resistance. However, the amount of carboplatin required to achieve this as a single-agent may be toxic for the host and thus not feasible. In contrast, combination therapy at low doses, with carboplatin administered optimally as described earlier, is sufficient to prevent the onset of resistance. When resistance to carboplatin is intrinsic, tumor remission is no longer feasible, but our model can be applied to identify dosing strategies that extend periods of disease-free survival. It has been proposed that the development of chemoresistance may result from insufficient exposure of tumor cells to drugs [33], and our simulations further accentuate the dangers of under-treatment.

The model presented in this article has the potential to accelerate the translation from 'bench-to-bedside' of novel therapeutics such as ABT-737, and to reduce the costs associated with drug development. However, the eventual clinical application of our model will require the validation of its predictions with further experiments. For instance, tumor xenograft growth inhibition experiments with varying doses of carboplatin and ABT-737 alone, and in combination would be extremely helpful in fine-tuning the functional responses of cancer cells to therapy. Measuring the relative constitutive expression levels of the Bcl-2 family would improve the accuracy of the quantitative description of the ABT-737-targeted intracellular apoptosis pathway. Detailed pharmacokinetic studies of ABT-737, which include the temporal dynamics of its intracellular concentration, would help in a better parameterization of our model. Finally, experimentally validating our model predictions relating to the optimal time of infusion of carboplatin when co-administered with ABT-737 could constitute a significant breakthrough in the treatment of ovarian cancers, and solid tumors in general.

A limitation of our approach is that while we have incorporated carboplatin-resistance by simulating a completely resistant cell line, in practice a human tumor may contain many different phenotypes of cells with varying levels of resistance to carboplatin, and sensitivities to ABT-737. Further, resistance to therapy can arise from multiple mechanisms. Consequently, in future versions of our model we will incorporate a greater diversity of cellular phenotypes. We also plan to include the administration of paclitaxel as a third drug in the combination chemotherapy of ovarian cancers, and replace ABT-737 with ABT-263, its orally available analogue currently under phase I clinical trials for the treatment of a number of solid tumors [34].



## **Acknowledgements**

The authors thank Dr. Marisa Eisenberg and Dr. Paul Hurtado for many helpful discussions.

## **Grant Support**

This research has been supported in part by the Mathematical Biosciences Institute at The Ohio State University and the NSF (grant DMS 0931642). This publication is based on work supported in part by Award No. KUK-C1-013-04, made by King Abdullah University of Science and Technology (KAUST). MMH was supported the BMBF GerontoSys initiative and HFSP.

## References

- [1] Roett MA, Evans P. Ovarian cancer: an overview. *Am Fam Physician* 2009 ;80:609–16.
- [2] Bookman MA. The addition of new drugs to standard therapy in the first-line treatment of ovarian cancer. *Ann Oncol* 2010;21:vii211-17.
- [3] Vasey PA. Resistance to chemotherapy in advanced ovarian cancer: mechanisms and current strategies. *Br J Cancer* 2003;89 Suppl 3:S23-8.
- [4] Bukowski RM, Ozols RF, Markman M. The management of recurrent ovarian cancer. *Semin Oncol* 2007;34:S1-15.
- [5] Galluzzi L, Senovilla L, Vitale I, et al. Molecular mechanisms of cisplatin resistance. *Oncogene* 2012;31:1869-8.
- [6] Siddik ZH. Cisplatin: mode of cytotoxic action and molecular basis of resistance. *Oncogene* 2003;22:7265-79.
- [7] Adams JM, Cory S. The Bcl-2 apoptotic switch in cancer development and therapy. *Oncogene* 2007;26:1324–37.
- [8] Liu JR, Fletcher B, Page C, Hu C, Nunez G, Baker V. Bcl-X<sub>L</sub> is expressed in ovarian carcinoma and modulates chemotherapyinduced apoptosis. *Gynecol Oncol* 1998;70:398–403.
- [9] Minn AJ, Rudin CM, Boise LH, Thompson CB. Expression of Bcl-X<sub>L</sub> can confer a multidrug resistance phenotype. *Blood* 1995;86:1903–10.

- [10] Williams J, Lucas PC, Griffith KA, et al. Expression of Bcl-X<sub>L</sub> in ovarian carcinoma is associated with chemoresistance and recurrent disease. *Gynecol Oncol* 2005;96:287–95.
- [11] Brotin E, Meryet-Figuere M, Simonin K, Duval RE, Villedieu M, Leroy-Dudal J, et al. Bcl-X<sub>L</sub> and MCL-1 constitute pertinent targets in ovarian carcinoma and their concomitant inhibition is sufficient to induce apoptosis. *Int J Cancer* 2010;126:885–95.
- [12] Villedieu M, Louis MH, Dutoit S. Absence of Bcl-X<sub>L</sub> down-regulation in response to cisplatin is associated with chemoresistance in ovarian carcinoma cells. *Gynecol Oncol* 2007;105:31–44.
- [13] Witham J, Valenti MR, De-Haven-Brandon AK, et al. The Bcl-2/Bcl-X<sub>L</sub> family inhibitor ABT-737 sensitizes ovarian cancer cells to carboplatin. *Clin Cancer Res* 2007;13:7191–8.
- [14] Jain HV, Meyer-Hermann M. The molecular basis of synergism between carboplatin and ABT-737 therapy targeting ovarian carcinomas. *Cancer Res* 2011;71:705–15.
- [15] El-Kareh AW, Labes RE, Secomb TW. Cell cycle checkpoint models for cellular pharmacology of paclitaxel and platinum drugs. *AAPS J* 2008;10:15–34.
- [16] El-Kareh AW, Secomb TW. A mathematical model for cisplatin cellular pharmacodynamics. *Neoplasia* 2003;5:161–9.
- [17] Jain HV, Nör JE, Jackson TL. Quantification of endothelial cell-targeted anti-Bcl-2 therapy and its suppression of tumor growth and vascularization. *Mol Cancer Ther* 2009;8:2926–36.

- [18] Jain HV, Nör JE, Jackson TL. Modeling the VEGF-Bcl-2-CXCL8 pathway in intratumoral angiogenesis. *Bull Math Biol* 2008;70:89–117.
- [19] Bonate PL. Modeling tumor growth in oncology. In: Bonate PL, Howard DR, editors. *Pharmacokinetics in drug development*, volume 3. New York: Springer Verlag; 2011. p. 1-11.
- [20] Panetta JC. A logistic model of periodic chemotherapy. *Appl Math Lett* 1995;8:83-6.
- [21] Panetta JC, Adam J. A mathematical model of cycle-specific chemotherapy. *Math Comput Model* 1995;22:67-82.
- [22] Panetta JC. A logistic model of periodic chemotherapy with drug resistance. *Appl Math Lett* 1997;10:123-7.
- [23] Jain HV, Byrne HM. Qualitative analysis of an integro-differential equation model of periodic chemotherapy. *Appl Math Lett* 2012;25:2132-6.
- [24] Whitecross KF, Alsop AE, Cluse LA, et al. Defining the target specificity of ABT-737 and synergistic antitumor activities in combination with histone deacetylase inhibitors. *Blood* 2009;113:1982-91.
- [25] Keyfitz BL, Keyfitz N. The McKendrick partial differential equation and its uses in epidemiological studies. *Math Comput Model* 1997;26:1-9.
- [26] Siddik ZH, Newell DR, Boxall FE, Harrap KR. The comparative pharmacokinetics of carboplatin and cisplatin in mice and rats. *Biochem Pharmacol* 1987;36:1925-32.
- [27] Bajaj G, Yeo Y. Drug delivery systems for intraperitoneal therapy. *Pharm Res* 2010;27:735-38.

- [28] Lukas G, Brindle SD, Greengard P. The route of absorption of intraperitoneally administered compounds. *J Pharmacol Exp Ther* 1971;178:562-66.
- [29] Siemann DW, The unique characteristics of tumor vasculature and preclinical evidence for its selective disruption by Tumor-Vascular Disrupting Agents, *Cancer Treat Rev* 2011;37:63-74.
- [30] Chou TC, Talalay P. Quantitative analysis of dose-effect relationships: the combined effects of multiple drugs or enzyme inhibitors. *Adv Enzyme Regul* 1984;22:27-55.
- [31] Despierre E, Lambrechts D, Neven P, Amant F, Lambrechts S, Vergote I. The molecular genetic basis of ovarian cancer and its roadmap towards a better treatment. *Gynecol Oncol* 2010;117:358-65.
- [32] Calvert AH, Newell DR, Gumbrell LA, O'Reilly S, Burnell M, Boxall FE, et al. Carboplatin dosage: prospective evaluation of a simple formula based on renal function. *J Clin Oncol* 1989;7:1748–56.
- [33] Tan DS, Ang JE, Kaye SB. Ovarian cancer: can we reverse drug resistance? *Adv Exp Med Biol* 2008;622:153-67.
- [34] Gandhi L, Camidge DR, Ribeiro de Oliveira M, et al. Phase I study of Navitoclax (ABT-263), a novel Bcl-2 family inhibitor, in patients with small-cell lung cancer and other solid tumors. *J Clin Oncol* 2011;29:909-16.

## Figure Legends

**Figure 1: A**, Model schematic. Ovarian cancer cells,  $N(t)$  proliferate and undergo apoptosis at a rate dependent on intracellular Bax concentration. Administration of carboplatin induces DNA damage, leading to cell cycle arrest. Arrested cells,  $M(t,a)$  subsequently undergo apoptosis at a rate proportional to the amount of DNA damage sustained at the time of arrest and on their intracellular Bax concentration, and may also recover to the proliferating population. The rates at which  $N$  and  $M$  undergo cell death are elevated on application of ABT-737, which leads to increased levels of intracellular Bax. **B**, Intracellular reaction diagram of the heterodimerization reaction between Bcl-X<sub>L</sub> ( $B$ ) and Bax ( $X$ ) molecules, and the inhibition of Bcl-X<sub>L</sub> by intracellular ABT-737 ( $A_C$ ). **C, D**, Fit to time-course tumor xenograft growth inhibition data taken from [13]. Briefly, ovarian cancer (IGROV-1 cell) xenografts were established in mice and treatment started 19 days post-transplantation. Levels of tumor growth inhibition were recorded periodically. Experimental data is represented by black squares and red triangles, while solid curves show best fits. Values represent mean and standard deviation (from experimental data). **C**, Weekly treatment with vehicle (black squares and curve) or daily treatment with 100 mg/kg of ABT-737 (red triangles and curve). **D**, Weekly treatment with 30 mg/kg carboplatin (black squares and curve) or a combination of carboplatin and ABT-737 (red triangles and curve).

**Figure 2: A**, Predicted Combination Index (CI) values computed for a desired tumor growth inhibition level of 67%, for various combinations of carboplatin and ABT-737. Following the experimental protocol in [13], treatment is initiated at 19 days post-transplantation and continued for 4 weeks. Simulations indicate that a combination of 17.8 mg/kg carboplatin given weekly combined with a daily dose of 86.5 mg/kg ABT-737 minimizes the CI and hence maximizes the synergy between the two drugs (dashed lines). **B**, Predicted tumor growth dynamics corresponding to the optimal dose combination found above. Plots show tumor cell numbers averaged over 7 days (the period of carboplatin administration) versus time. **C**,

Predicted time-courses of tumor growth inhibition levels as compared to the control (no treatment) case, corresponding to the optimal dose combination found above.

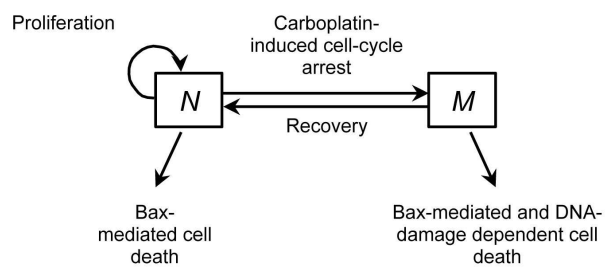
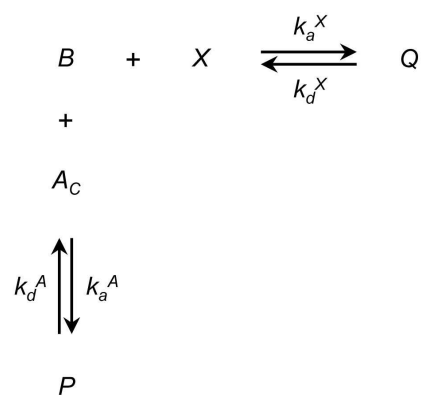
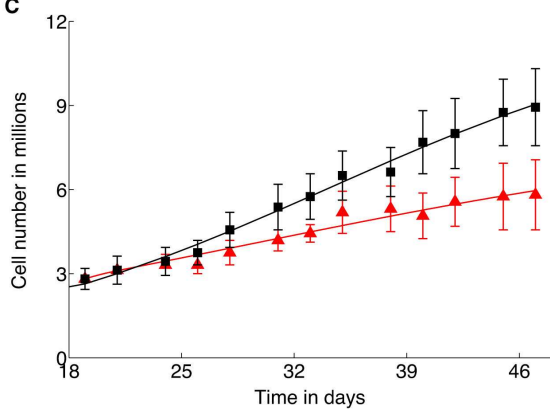
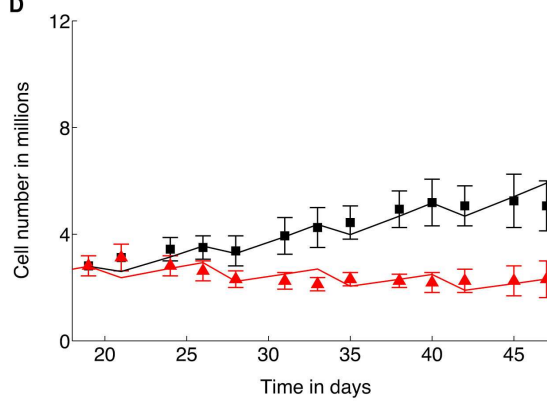
**Figure 3:** Simulations showing long-term tumor xenograft response to combination therapy. Following the experimental protocol in [13], the administration of a weekly dose of 30 mg/kg carboplatin together with a daily dose of 100 mg/kg ABT-737 is simulated, and simulations allowed to run until tumor cell numbers averaged over 7 days (the period of carboplatin administration) achieve a steady-state. **A**, Predicted steady states of average tumor cell numbers as a function of carboplatin infusion time  $T_i$ . As  $T_i$  is increased from 0 hours (corresponding to a bolus dose) to 120 hours, the average tumor cell number steady-state decreases rapidly to  $< 1$  (see inset), and then increases, with minimal survival of tumor cells predicted for  $1 \leq T_i \leq 25$ . **B**, Predicted values of  $T_m$ , the length of time therapy must be administered to achieve minimal residual disease (defined as  $< 1$  cell remaining) as  $T_i$  is varied between 1 and 25 hours. A minimum value of  $T_m = 215$  days is predicted for weekly carboplatin infusions lasting 8 hours. **C**, Minimum values of  $T_m$  are predicted to decrease to 215 days as  $\rho_s$ , the arrested cell sensitivity to intracellular Bax is increased. In all cases, a carboplatin infusion time of 8 hours minimized the cure time.

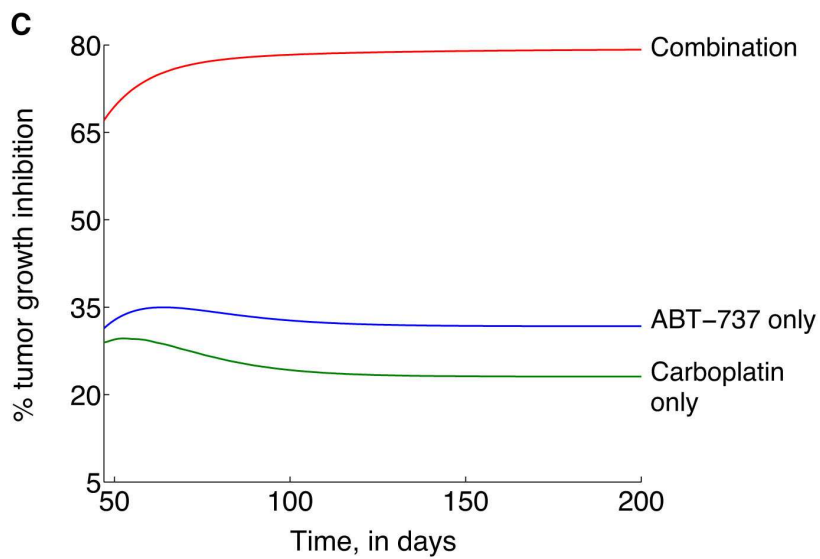
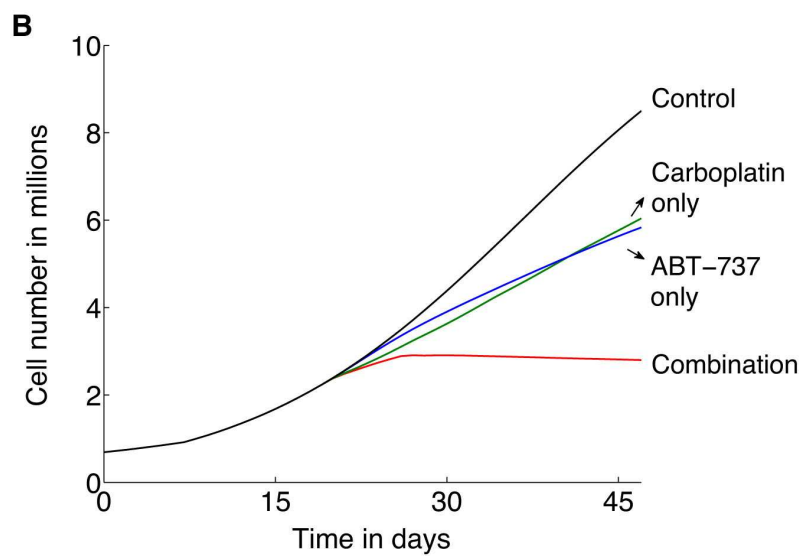
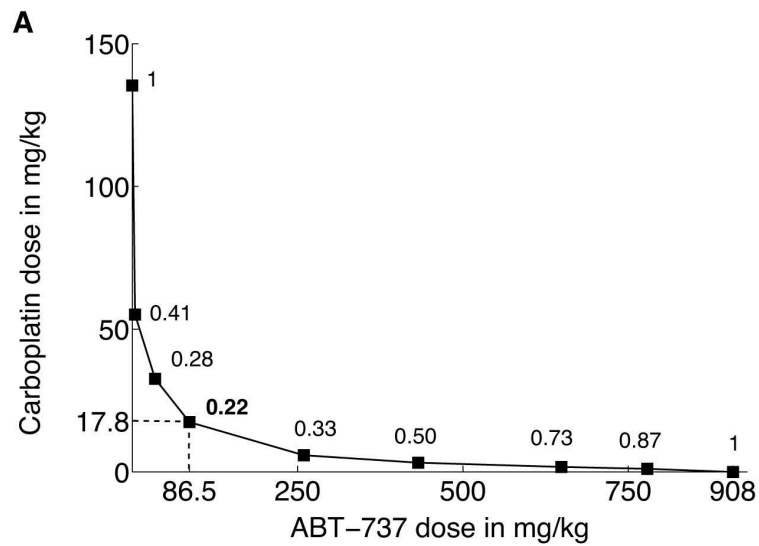
**Figure 4:** The emergence of acquired resistance to carboplatin therapy, where DNA-mismatch repair in arrested cells recovering to the proliferating population is assumed to be the cause of resistance. The treatment of a late-stage tumor is simulated. Plots show 7 day-averages of carboplatin-sensitive (blue curve), carboplatin-resistant (red curve) and total (dashed black curve) tumor cell numbers versus time, as treatment strategy is varied. In all cases, therapy is administered for a period of 1 year. Increasing the weekly bolus dose of carboplatin administered as a single agent from **A**, 30 mg/kg, **B**, 300 mg/kg, to **C**, 800 mg/kg, cannot prevent the emergence of carboplatin-resistance. **D**, In fact, a weekly dose of 1300 mg/kg carboplatin is required to induce tumor regression. **E**, A combination of 30 mg/kg carboplatin

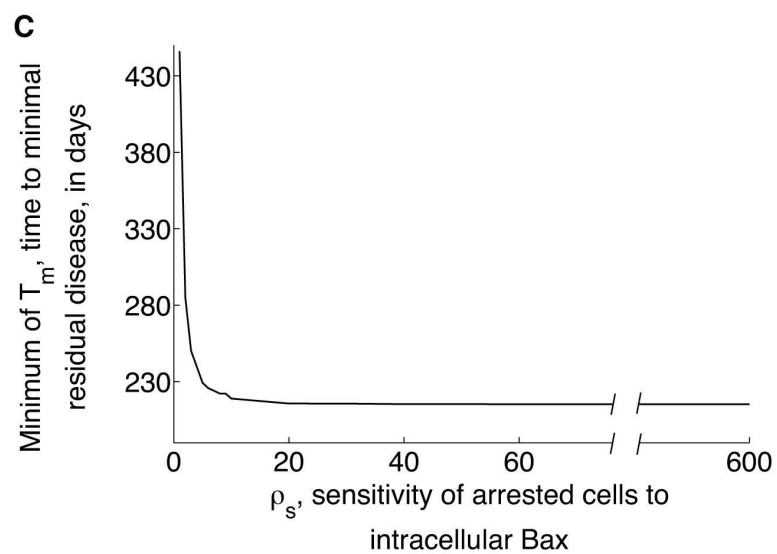
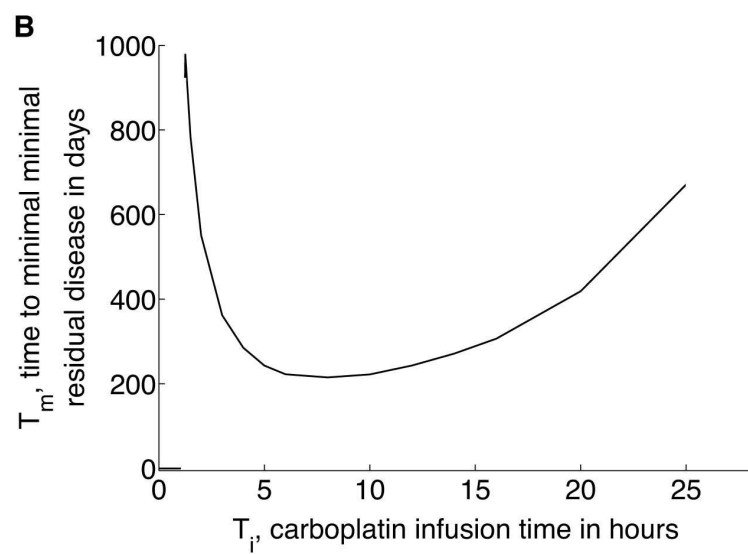
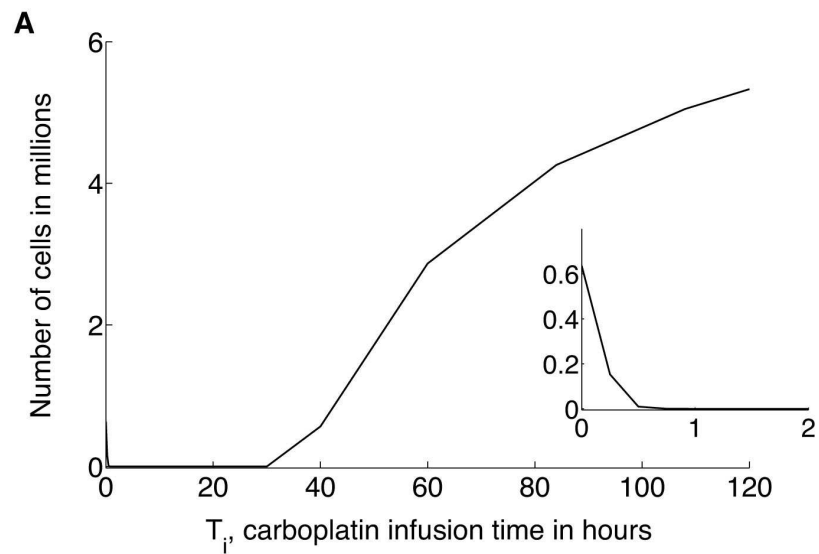
delivered weekly as a bolus together with 100 mg/kg ABT-737 delivered daily is predicted to prevent the emergence of resistance and lead to tumor growth control at 6.5% of pre-treatment levels. **F**, The same combination dose, with carboplatin delivered via a 8-hour infusion is predicted to induce tumor regression within 150 days.

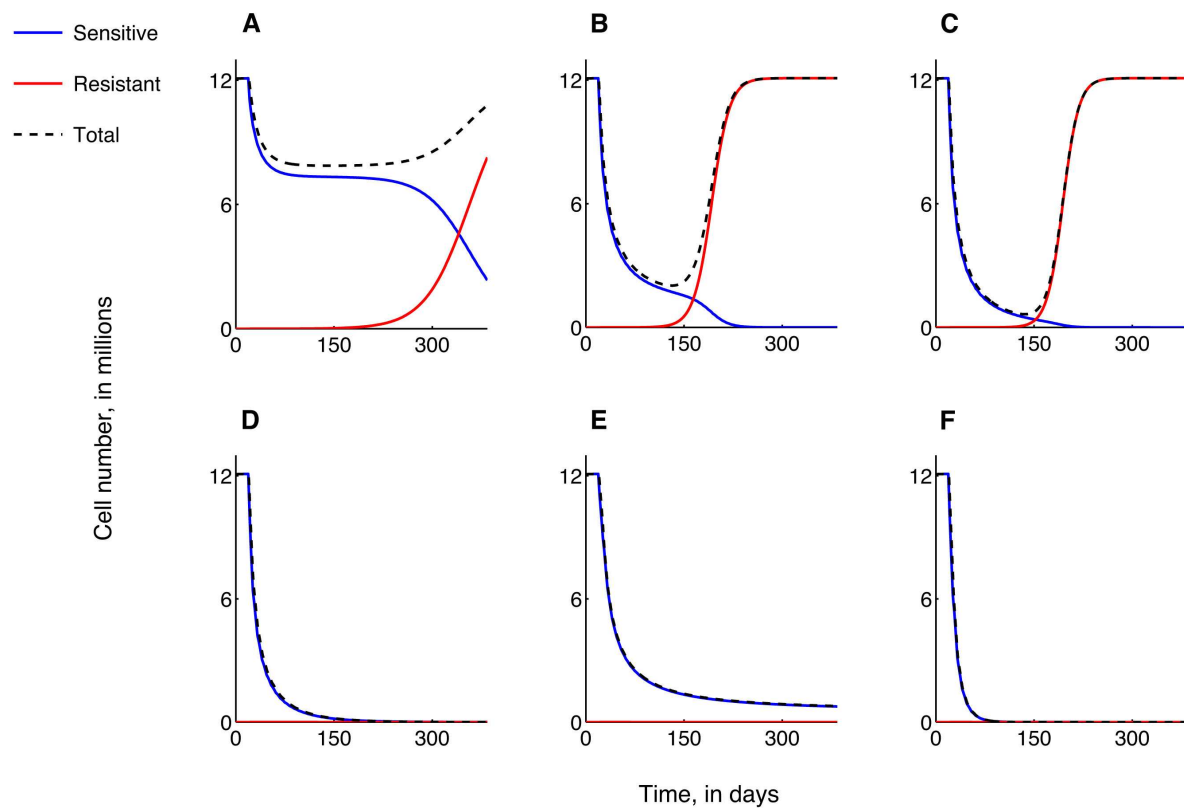
**Figure 5:** Intrinsic resistance to carboplatin therapy, where a small fraction (1 in 60,000) of carboplatin-resistant cells is assumed to be present prior to treatment initiation. The treatment of a late-stage tumor is simulated. Plots show 7 day-averages of carboplatin-sensitive (blue curve), carboplatin-resistant (red curve) and total (dashed black curve) tumor cell numbers versus time, as treatment strategy is varied. In all cases, therapy is administered for a period of 1 year. Increasing the weekly bolus dose of carboplatin administered as a single agent from **A**, 30 mg/kg, **B**, 600 mg/kg, to **C**, 1300 mg/kg, cannot prevent the onset of carboplatin-resistance, with overall tumor size returning to pre-treatment levels eventually. **D**, **E**, **F**, In fact, a combination therapy of 30 mg/kg carboplatin delivered weekly as a bolus (**D**) or via 8-hour infusion (**E**, **F**) together ABT-737 delivered daily at a dose of 100 mg/kg (**D**, **E**) or 500 mg/kg (**F**) is also unable to prevent the emergence of resistance. However, combination therapy is predicted to result in partial tumor growth control, with a steady-state tumor size reaching 65.2% of pre-treatment levels for a combination of 30 mg/kg carboplatin and 100 mg/kg ABT-737 (**D**, **E**). Increasing ABT-737 dosage to 500 mg/kg is predicted to induce extended periods of disease-free survival, as evidenced by a dip in the total tumor size graph (**F**).

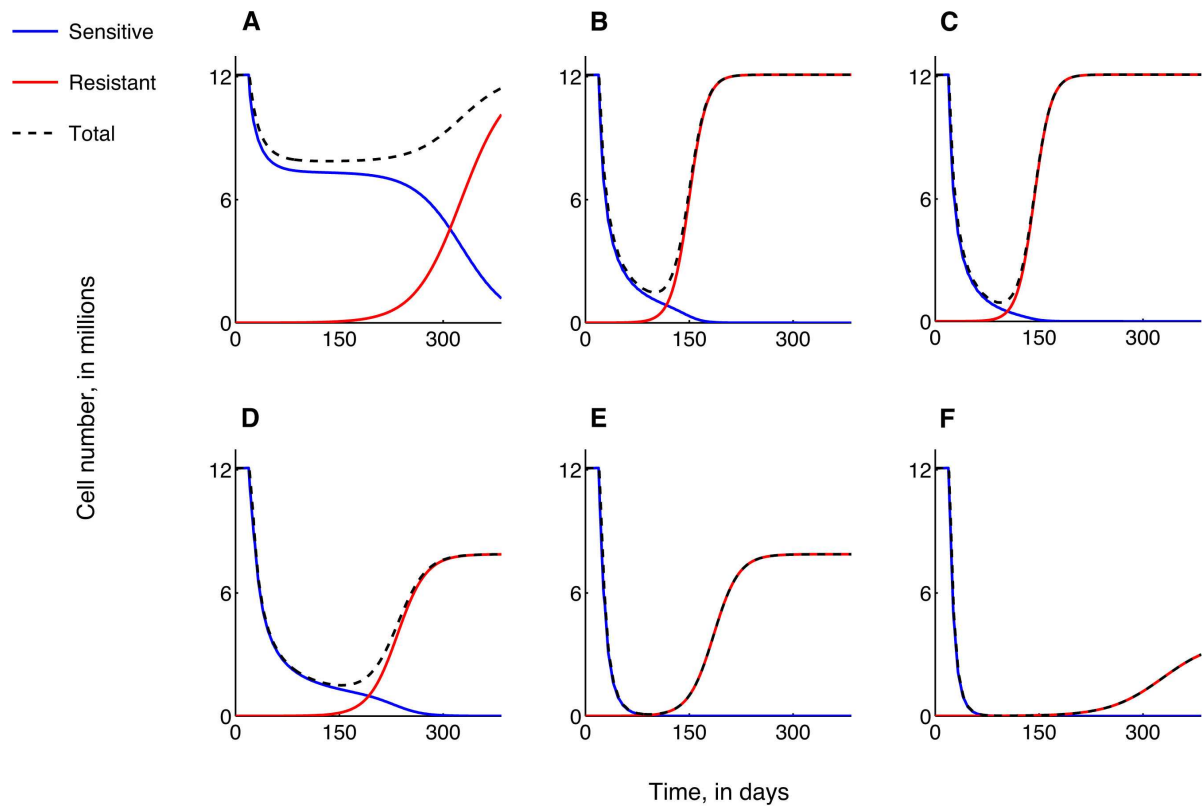


**A****B****C****D**









# Supplementary Information

## S1 Model Equations

The full system of equations used to model the treatment with carboplatin and ABT-737 of an ovarian cancer xenograft is presented below, together with notation used.

### Notation

$t$	Time (days)
$a$	Time (days)
$N(t)$	Number of carboplatin-sensitive proliferating ovarian cancer cells (millions)
$M(t, a)$	Number of arrested cancer cells that have spent time $a$ in the arrested state (millions/day)
$C_{perit}(t)$	Intraperitoneal carboplatin concentration ( $\mu\text{M}$ )
$C_P(t)$	Plasma carboplatin concentration ( $\mu\text{M}$ )
$C_T(t)$	Tissue carboplatin concentration ( $\mu\text{M}$ )
$A_{perit}(t)$	Intraperitoneal ABT-737 concentration (nM)
$A_P(t)$	Plasma ABT-737 concentration (nM)
$A_C(t)$	Intracellular ABT-737 concentration (nM)
$B(t)$	Intracellular Bcl-X <sub>L</sub> concentration (nM)
$X(t)$	Intracellular Bax concentration (nM)
$P(t)$	Intracellular Bcl-X <sub>L</sub> -ABT-737 complex concentration (nM)
$Q(t)$	Intracellular Bcl-X <sub>L</sub> -Bax complex concentration (nM)

### Proliferating Cell Equation

$$\frac{dN}{dt} = \underbrace{\lambda_N N \left( 1 - \frac{N + \int_{t-a_r}^t M(t, a) da}{K} \right)}_{\text{logistic growth}} - \underbrace{\delta_N(X) N}_{\text{Bcl-X}_L\text{-mediated cell death}} - \underbrace{\alpha_C(C_T) N}_{\text{carboplatin-induced cell arrest}} + \underbrace{M(t, a = a_r)}_{\text{recovery to proliferating pool}}, \quad (\text{S1.1})$$

with initial condition  $N(t = 0) = 0.69$  million cells.

### Arrested Cell Equation

$$\frac{\partial M}{\partial t} + \frac{\partial M}{\partial a} = - \underbrace{\delta_M(C_T(t-a), X(t), a) M}_{\text{Bcl-X}_L\text{- and carboplatin-mediated arrested cell death}}, \quad (\text{S1.2})$$

with boundary condition

$$M(t, 0) = \alpha_C(C_T) N, \quad (\text{S1.3})$$

and with initial condition  $M(t = 0, a) = 0$  million cells per day.

### Carboplatin Pharmacokinetics

$$\frac{dC_{perit}}{dt} = \underbrace{-\mu_C C_{perit}}_{\text{extravasation to systemic circulation}} + \underbrace{K_0(T_i) H(T_i - t)}_{\text{dosage with time of infusion } T_i}, \quad (\text{S1.4})$$

$$\frac{dC_P}{dt} = \underbrace{\mu_C \frac{V_{perit}^C}{V_P^C} C_{perit}}_{\text{source from peritoneal cavity}} - \underbrace{K_C C_P}_{\text{clearance}} - \underbrace{K_{PT}^C C_P}_{\text{extravasation to peripheral tissue}} + \underbrace{K_{TP}^C \frac{V_T^C}{V_P^C} C_T}_{\text{source from peripheral tissue}}, \quad (\text{S1.5})$$

$$\frac{dC_T}{dt} = \underbrace{K_{PT}^C \frac{V_P^C}{V_T^C} C_P}_{\text{source from systemic circulation}} - \underbrace{K_{TP}^C C_T}_{\text{extravasation to systemic circulation}}, \quad (\text{S1.6})$$

with initial conditions  $C_{perit}(t = 0) = C_P(t = 0) = C_T(t = 0) = 0$   $\mu\text{M}$ .

### ABT-737 Pharmacokinetics and Intracellular Signal Transduction

$$\frac{dA_{perit}}{dt} = \underbrace{-\mu_A A_{perit}}_{\text{extravasation to systemic circulation}}, \quad (\text{S1.7})$$

$$\frac{dA_P}{dt} = \underbrace{\mu_A \frac{V_{perit}^A}{V_P^A} A_{perit}}_{\text{source from peritoneal cavity}} - \underbrace{K_A A_P}_{\text{clearance}} - \underbrace{K_{PC}^A A_P}_{\text{extravasation to intra-cellular compartment}} + \underbrace{K_{CP}^A \frac{V_C^A}{V_P^A} A_C}_{\text{source from intra-cellular compartment}}, \quad (\text{S1.8})$$

$$\frac{dA_C}{dt} = \underbrace{-k_a^A A_C B + k_d^A P}_{\text{reaction with Bcl-X}_L} + \underbrace{K_{PC}^A \frac{V_P^A}{V_C^A} A_P}_{\text{source from systemic circulation}} - \underbrace{K_{CP}^A A_C}_{\text{extravasation to systemic circulation}}, \quad (\text{S1.9})$$

$$\frac{dB}{dt} = \underbrace{-k_a^A A_C B + k_d^A P}_{\text{reaction with ABT-737}} - \underbrace{k_a^X X B + k_d^X Q}_{\text{reaction with Bax}}, \quad (\text{S1.10})$$

$$\frac{dX}{dt} = \underbrace{-k_a^X X B + k_d^X Q}_{\text{reaction with Bcl-X}_L}, \quad (\text{S1.11})$$

$$\frac{dP}{dt} = \underbrace{k_a^A A_C B - k_d^A P}_{\text{ABT-737-Bcl-X}_L \text{ reaction}}, \quad (\text{S1.12})$$

$$\frac{dQ}{dt} = \underbrace{k_a^X X B - k_d^X Q}_{\text{Bax-Bcl-X}_L \text{ reaction}}, \quad (\text{S1.13})$$

with initial conditions  $A_{perit}(t=0) = A_P(t=0) = A_C(t=0) = 0$  nM;  $B(t=0) = 75$  nM;  $X(t=0) = 83.33$  nM; and  $P(t=0) = Q(t=0) = 0$  nM.

In the above equations, the Bax-dependent death rate of proliferating cells is

$$\delta_N(X) = r_X X; \quad (\text{S1.14})$$

the rate of proliferating cell arrest induced by carboplatin is

$$\alpha_C(C_T) = r_C \frac{C_T^2}{C_T^2 + K_{carb}^2}; \quad (\text{S1.15})$$

the carboplatin- and Bax-dependent rate of arrested cell death is

$$\delta_M(C_T(t-a), X(t), a) = (\rho_C + \rho_S r_X (X - X_{phys})) C_T(t-a) H(a - a_{char}); \quad (\text{S1.16})$$



the carboplatin infusion dosage function is

$$K_0(T_i) = \begin{cases} 0, & \text{if } T_i = 0 \\ D_C / (V_{perit}^C w_C T_i), & \text{if } T_i > 0 \end{cases}; \quad (\text{S1.17})$$

and the Heaviside function is defined as

$$H(x) = \begin{cases} 0, & \text{if } x \leq 0 \\ 1, & \text{if } x > 0 \end{cases}. \quad (\text{S1.18})$$

In the sections that follow, we explain how the model equations were developed, discuss parameter estimates and outline the simulation methodology used to generate the numerical results.

### S1.1 Modeling resistance to carboplatin

Carboplatin-resistant cells are denoted with the variable  $R(t)$ . They are assumed to be insensitive to treatment with carboplatin, but as sensitive to ABT-737 as  $N$  cells. In our model, the following two cases are considered: (i) acquired resistance where cells recovering from a carboplatin-induced state of arrest experience aberrant DNA damage repair, resulting in a resistant phenotype, and (ii) intrinsic resistance where a small population of resistant cells is present initially. The equations governing the evolution of  $N$  and  $R$  cell dynamics for the two cases of interest are presented below.

#### Acquired resistance

$$\frac{dN}{dt} = \lambda_N N \left(1 - \frac{T}{K}\right) - \delta_N(X) N - \alpha_C(C_T) N + p M(t, a = a_r), \quad (\text{S1.19})$$

$$\frac{dR}{dt} = \lambda_R R \left(1 - \frac{T}{K}\right) - \delta_R(X) R + (1 - p) M(t, a = a_r), \quad (\text{S1.20})$$

subject to initial conditions  $N(t = 0) = 12.08$  million cells and  $R(t = 0) = 0$  million cells, and where  $T(t) = N(t) + R(t) + \int_{t-a_r}^t M(t, a) da$  is the total number of cells at time  $t$  and  $p$  is the probability of aberrant DNA damage repair.

### Intrinsic resistance

$$\frac{dN}{dt} = \lambda_N N \left(1 - \frac{T}{K}\right) - \delta_N(X) N - \alpha_C(C_T) N + M(t, a = a_r), \quad (\text{S1.21})$$

$$\frac{dR}{dt} = \lambda_R R \left(1 - \frac{T}{K}\right) - \delta_R(X) R, \quad (\text{S1.22})$$

subject to initial conditions  $N(t = 0) = 12.078$  million cells and  $R(t = 0) = 0.002$  million cells, and where, as before,  $T(t) = N(t) + R(t) + \int_{t-a_r}^t M(t, a) da$  is the total number of cells at time  $t$ .

In equations (S1.20) and (S1.22), the Bax-dependent death rate of resistant cell death is taken as

$$\delta_R(X) = r_X X. \quad (\text{S1.23})$$

## **S2 ABT-737 Pharmacokinetics and the Intracellular Regulation of Cell Death**

In this section we explain how we model ABT-737 pharmacokinetics and pharmacodynamics.

### **S2.1 Model Derivation**

In experiments described in [1], ABT-737 (an 813 Da compound) is administered intraperitoneally via periodic bolus injections. The following 3-compartment model is assumed to govern its pharmacokinetics and a schematic is shown in Figure S1A. The first compartment is the peritoneal cavity into which the drug is injected. Experimental evidence suggests that small molecular weight drugs are readily absorbed through the peritoneal vasculature from here they enter the systemic circulation [2, 3], which is taken to be the second compartment. From here the drug may be cleared from the body, or enter the third, intracellular compartment where it interacts with the Bcl-2 family of proteins (specifically, Bax and

Bcl-X<sub>L</sub>), as represented by the following reactions:



Here,  $k_a^A$  and  $k_a^X$  are the association rate constants for Bcl-X<sub>L</sub> binding ABT-737 and Bax respectively, and  $k_d^A$  and  $k_d^X$  are the corresponding dissociation rate constants. By appealing to the principal of mass balance, these reactions may be translated into a system of time-dependent differential equations describing how the concentrations of intracellular ABT-737, Bax, Bcl-X<sub>L</sub>, ABT-737-Bcl-X<sub>L</sub> complex and Bax-Bcl-X<sub>L</sub> vary with time. It is straightforward to show that the complete system of equations governing the pharmacokinetics and intracellular dynamics of ABT-737 is given by:

$$\frac{dA_{perit}}{dt} = -\mu_A A_{perit}, \quad (S2.1)$$

$$\frac{dA_P}{dt} = \mu_A \frac{V_{perit}^A}{V_P^A} A_{perit} - K_A A_P - K_{PC}^A A_P + K_{CP}^A \frac{V_C^A}{V_P^A} A_C, \quad (S2.2)$$

$$\frac{dA_C}{dt} = -k_a^A A_C B + k_d^A P + K_{PC}^A \frac{V_P^A}{V_C^A} A_P - K_{CP}^A A_C, \quad (S2.3)$$

$$\frac{dB}{dt} = -k_a^A A_C B + k_d^A P - k_a^X X B + k_d^X Q, \quad (S2.4)$$

$$\frac{dP}{dt} = k_a^A A_C B - k_d^A P, \quad (S2.5)$$

$$\frac{dX}{dt} = -k_a^X X B + k_d^X Q, \quad (S2.6)$$

$$\frac{dQ}{dt} = k_a^X X B - k_d^X Q. \quad (S2.7)$$

Here,  $A_{perit}(t)$ ,  $A_P(t)$  and  $A_C(t)$  represent the concentrations of ABT-737 in the peritoneal, circulatory and intracellular compartments, respectively;  $V_{perit}^A$ ,  $V_P^A$  and  $V_C^A$  are the assumed constant volumes of

distribution of ABT-737 in these compartments; and  $\mu_A$  is the rate of extravasation of ABT-737 from the peritoneal cavity into the systemic circulation,  $K_A$  is the rate of its clearance from circulation; and  $K_{PC}^A$  and  $K_{CP}^A$  are the rates of entry of ABT-737 from the systemic circulation into the intracellular compartment and vice versa, respectively. In the absence of additional information, we assume  $V_{perit}^A \approx V_P^A \approx V_C^A$ . Equation (S2.1) can be solved explicitly to give  $A_{perit}(t) = \alpha_{perit} e^{-\mu_A t}$ , where  $\alpha_{perit} = A_{perit}(t=0)$ . When simulating the periodic administration of the drug (with period  $\tau_A \geq 1$  day), the expression for the intraperitoneal concentration of ABT-737 is modified to  $A_{perit}(t) = \alpha_{perit} e^{-\mu_A rem(t, \tau_A)}$ , where  $rem(x, y)$  denotes the remainder when  $x$  is divided by  $y$ . We remark that equations (S2.4)-(S2.7) imply the following conservation laws for intracellular Bcl-X<sub>L</sub> and Bax:

$$B(t) + P(t) + Q(t) = \beta \quad \text{and} \quad X(t) + Q(t) = \chi, \quad (\text{S2.8})$$

where  $\beta$  and  $\chi$  are positive constants representing the total amounts in a given cell of Bcl-X<sub>L</sub> and Bax, respectively.

## S2.2 Parameter Estimation

A list of parameter values with sources is provided in Table S1. For clarity, we discuss the estimation of those parameters values which could not be determined directly from the literature. Since we require that ABT-737 is cleared from the peritoneal cavity within 24 hours (see previous subsection), we estimate that  $\mu_A$ , its rate of extravasation from the peritoneal cavity into the systemic circulation, satisfies  $\mu_A \geq 5.30$  per day. Here we take  $\mu_A = 6$  per day. The rate  $K_{CP}^A$  of ABT-737 leakage from the intracellular compartment to the circulation, and its rate  $K_{PC}^A$  of entry from the circulation to the intracellular compartment are chosen to ensure that the intracellular concentration of ABT-737 is comparable to typical expression levels of the Bcl-2 family of proteins (estimated to be of the order of a few nM [4, 5]).

Equations (S2.1)-(S2.7) are simulated using the parameter values in Table S1 to generate typical ABT-737, Bcl-X<sub>L</sub> and Bax time-courses, for a therapy schedule in which 100 mg/kg ABT-737 is given daily, the first treatment time at  $t = 5$  days. The results presented in Figure S1 reveal that ABT-737 is rapidly

cleared from the peritoneal cavity after each dose (Figure S1B). Correspondingly, ABT-737 levels in the systemic circulation settle to periodic oscillations, with a maximum of  $5.9 \mu\text{M}$  and a minimum of  $0.9 \mu\text{M}$  (see Figure S2C). The intracellular ABT-737 concentration is also periodic with a maximum of  $4.5 \text{ nM}$  and a minimum of  $4.0 \text{ nM}$  (see Figure S2D). Prior to therapy, the intracellular concentrations of Bcl-X<sub>L</sub> and Bax are at their steady state values of  $19.83$  and  $27.83 \text{ nM}$ , respectively (see Figure S2E). When therapy is administered, the Bcl-X<sub>L</sub> concentration falls rapidly, eventually oscillating between values of  $7.3$  and  $7.8 \text{ nM}$ , while the Bax concentration rises and undergoes periodic solutions with levels ranging from  $46.7$  and  $48.0 \text{ nM}$ . The period of the oscillations in the intracellular levels of ABT-737, Bcl-X<sub>L</sub> and Bax correspond to the period of drug administration (1 day), with ABT-737 and Bax oscillating in phase, and Bcl-X<sub>L</sub> oscillating  $\pi$  radians out of phase. This phase shift is a result of the inhibitory action of ABT-737 on Bcl-X<sub>L</sub>.

### S2.3 Asymptotic Analysis

The parameter estimates in Table S1 reveal that equations (S2.1)-(S2.7) operate on multiple different time scales. We now conduct an asymptotic analysis of these equations in order to understand the system dynamics on the longer time-scale that corresponds to therapy application and tumor growth. The system of equations is first recast in dimensionless variables, which are denoted with an asterisk. The following rescaling is chosen:  $A_{perit}^* = A_{perit}/\alpha_{perit}$ ,  $A_P^* = A_P/\alpha_P$  where  $\alpha_P = \max_{t \in [0, \infty)} A_P(t)$ ,  $A_C^* = A_C/\alpha_C$  where  $\alpha_C = \max_{t \in [0, \infty)} A_C(t)$ ,  $B^* = B/\beta$ ,  $P^* = P/\beta$ ,  $Q^* = Q/\beta$  and  $X^* = X/\chi$ . Finally, time is scaled with the timescale associated with consecutive applications of therapy so that  $t^* = t/\tau_A$ . Introducing these variables in equations (S2.1)-(S2.7) (and omitting asterisks for ease of notation), we obtain the following non-dimensional system.

$$A_{perit}(t) = e^{-\bar{\mu}_A rem(t,1)}, \quad (\text{S2.9})$$

$$\frac{dA_P}{dt} = \bar{\eta}_A A_{perit} - \bar{K}_A A_P - \epsilon \bar{\kappa}_0 (\bar{\kappa}_1 A_P - \bar{\kappa}_2 A_C), \quad (\text{S2.10})$$

$$\epsilon \frac{dA_C}{dt} = -\bar{\gamma}_1 (\bar{\nu}_1 A_C B - \bar{\nu}_2 P) + \epsilon (\bar{\kappa}_1 A_P - \bar{\kappa}_2 A_C), \quad (\text{S2.11})$$

$$\epsilon \frac{dB}{dt} = -(\bar{\nu}_1 A_C B - \bar{\nu}_2 P) - (\bar{\nu}_3 X B - Q), \quad (\text{S2.12})$$

$$\epsilon \frac{dX}{dt} = -\bar{\gamma}_2 (\bar{\nu}_3 X B - Q), \quad (\text{S2.13})$$

where  $P = 1 - B - Q$  and  $Q = (1 - X)/\bar{\gamma}_2$  from the conservation laws stated in (S2.8).

We have introduced a small parameter  $\epsilon = 1/(k_d^X \tau_A)$ , which measures the ratio of the frequency of ABT-737 application, and the dissociation rate of the Bcl-X<sub>L</sub>-Bax complex into its constituent species. The non-dimensional parameters (denoted by an overbar in the above equations) are defined in Table S2.

We approximate solutions of the model variables which are regular power series expansions in  $\epsilon$  so that, for example,

$$A_P(t) = A_{P,0}(t) + \epsilon A_{P,1}(t) + \epsilon^2 A_{P,2}(t) + \dots$$

Substituting the above into equation (S2.10) gives:

$$\begin{aligned} \frac{d}{dt} (A_{P,0} + \epsilon A_{P,1}) &= \bar{\eta}_A A_{perit} - \bar{K}_A (A_{P,0} + \epsilon A_{P,1}) - \epsilon \bar{\kappa}_0 \bar{\kappa}_1 (A_{P,0} + \epsilon A_{P,1}) \\ &\quad + \epsilon \bar{\kappa}_0 \bar{\kappa}_2 (A_{C,0} + \epsilon A_{C,1}) + O(\epsilon^2). \end{aligned} \quad (\text{S2.14})$$

Equating coefficients of  $O(\epsilon^0)$  and  $O(\epsilon^1)$  we get:

$$\frac{dA_{P,0}}{dt} = \bar{\eta}_A A_{perit} - \bar{K}_A A_{P,0}, \quad (\text{S2.15})$$

$$\frac{dA_{P,1}}{dt} = -\bar{K}_A A_{P,1} - \bar{\kappa}_0 \bar{\kappa}_1 A_{P,0} + \bar{\kappa}_0 \bar{\kappa}_2 A_{C,0}. \quad (\text{S2.16})$$

The same process applied to equations (S2.11)-(S2.13) gives:

$$0 = -\bar{\nu}_1 A_{C,0} B_0 + \bar{\nu}_2 P_0, \quad (\text{S2.17})$$

$$0 = -\bar{\nu}_3 X_0 B_0 + Q_0, \quad (\text{S2.18})$$

$$\frac{dA_{C,0}}{dt} = -\bar{\gamma}_1 (\bar{\nu}_1 A_{C,0} B_1 + \bar{\nu}_1 A_{C,1} B_0 - \bar{\nu}_2 P_1) + (\bar{\kappa}_1 A_{P,0} - \bar{\kappa}_2 A_{C,0}), \quad (\text{S2.19})$$

$$\frac{dB_0}{dt} = -(\bar{\nu}_1 A_{C,0} B_1 + \bar{\nu}_1 A_{C,1} B_0 - \bar{\nu}_2 P_1) - (\bar{\nu}_3 X_0 B_1 + \bar{\nu}_1 X_1 B_0 - Q_1), \quad (\text{S2.20})$$

$$\frac{dX_0}{dt} = -\bar{\gamma}_2 (\bar{\nu}_3 X_0 B_1 + \bar{\nu}_1 X_1 B_0 - Q_1), \quad (\text{S2.21})$$

where  $P_0 = 1 - B_0 - Q_0$  and  $Q_0 = (1 - X_0)/\bar{\gamma}_2$ . Equations (S2.17) and (S2.18) may be solved simultaneously to obtain the following expressions for  $B_0$  and  $X_0$  in terms of  $A_{C,0}$ :

$$B_0(A_{C,0}) = \frac{-(\zeta_1 A_{C,0} + \zeta_2) + \zeta_1 \sqrt{A_{C,0}^2 + \rho_1 A_{C,0} + \rho_2}}{\bar{\nu}_1 A_{C,0} + \bar{\nu}_2}, \quad (\text{S2.22})$$

$$X_0(A_{C,0}) = -(\sigma_1 A_{C,0} + \sigma_2) + \sigma_1 \sqrt{A_{C,0}^2 + \rho_1 A_{C,0} + \rho_2}. \quad (\text{S2.23})$$

The new parameters  $\zeta_i, \sigma_i, \rho_i$  ( $i = 1, 2$ ) are defined in Table S2. Further, from equations (S2.19)-(S2.21), we deduce

$$\frac{dA_{C,0}}{dt} = \bar{\gamma}_1 \left( \frac{dB_0}{dt} - \frac{1}{\bar{\gamma}_2} \frac{dX_0}{dt} \right) + (\bar{\kappa}_1 A_{P,0} - \bar{\kappa}_2 A_{C,0}). \quad (\text{S2.24})$$

Finally, a simplified differential equation for  $A_{C,0}$  is obtained by substituting equations (S2.22) and (S2.23) into equation (S2.24). Finally, by neglecting terms of  $O(\epsilon)$ , we obtain the following approximation (in non-dimensional terms) to equations (S2.1)-(S2.7) which model ABT-737 pharmacokinetics and intra-

cellular dynamics, on the timescale of tumor growth.

$$A_{perit}(t) = e^{-\bar{\mu}_A rem(t,1)}, \quad (\text{S2.25})$$

$$\frac{dA_P}{dt} = \bar{\eta}_A A_{perit} - \bar{K}_A A_P, \quad (\text{S2.26})$$

$$B(A_C) = \frac{-(\zeta_1 A_C + \zeta_2) + \zeta_1 \sqrt{A_C^2 + \rho_1 A_C + \rho_2}}{\bar{\nu}_1 A_C + \bar{\nu}_2}, \quad (\text{S2.27})$$

$$X(A_C) = -(\sigma_1 A_C + \sigma_2) + \sigma_1 \sqrt{A_C^2 + \rho_1 A_C + \rho_2}, \quad (\text{S2.28})$$

$$\frac{dA_C}{dt} = (\bar{\kappa}_2 A_P - \bar{\kappa}_3 A_C) \frac{\bar{\gamma}_2}{\bar{\gamma}_2 - \bar{\gamma}_1 \bar{\gamma}_2 (dB/dA_C) + \bar{\gamma}_1 (dX/dA_C)}. \quad (\text{S2.29})$$

We remark that numerical validation of the above analysis is provided by the excellent agreement between the solutions of the original system of equations (S2.1)-(S2.7) and those of the reduced system (S2.25)-(S2.29) (see Figure S1F).

### S3 Carboplatin Pharmacokinetics

In this section, we explain how we model carboplatin pharmacokinetics.

#### S3.1 Model Derivation

In experiments described in [1], carboplatin is administered as a series of periodic intraperitoneal injections (or bolus doses). The following 3-compartment model is assumed to govern its pharmacokinetics and a schematic is shown in Figure S2A. As for ABT-737, the peritoneal cavity is the first compartment of interest. From here the drug extravasates into the systemic circulation, the second compartment. Experimental evidence suggests a biphasic plasma concentration-time curve for carboplatin [6]. Consequently, a third compartment, comprising tissues and organs with poor vascular perfusion, is also



included. Combining these effects, we deduce that the equations governing carboplatin pharmacokinetics are

$$\frac{dC_{perit}}{dt} = -\mu_C C_{perit} + K_0(T_i) H(T_i - t), \quad (S3.1)$$

$$\frac{dC_P}{dt} = \mu_C \frac{V_{perit}^C}{V_P^C} C_{perit} - K_C C_P - K_{PT}^C C_P + K_{TP} \frac{V_T^C}{V_P^C} C_T, \quad (S3.2)$$

$$\frac{dC_T}{dt} = K_{PT}^C \frac{V_P^C}{V_T^C} C_P - K_{TP}^C C_T. \quad (S3.3)$$

Here,  $C_{perit}(t)$ ,  $C_P(t)$  and  $C_T(t)$  are the concentrations of carboplatin in the peritoneal, circulatory and intracellular compartments, respectively;  $V_{perit}^C$ ,  $V_P^C$  and  $V_T^C$  are the assumed constant volumes of distribution of carboplatin in these compartments;  $\mu_C$  is the rate of extravasation of carboplatin from the peritoneal cavity into the systemic circulation;  $K_C$  is the rate of its clearance from circulation; and  $K_{PT}^C$  and  $K_{TP}^C$  represent the rates of entry of carboplatin from the systemic circulation into the intracellular compartment and vice versa. We consider several delivery strategies for carboplatin, including bolus and continuous infusions. The parameter  $T_i$  measures the infusion time of carboplatin with  $T_i = 0$  corresponding to a bolus dose. The function  $K_0(T_i)$  is the rate of infusion, defined as:

$$K_0(T_i) = \begin{cases} 0, & \text{if } T_i = 0, \\ R_i / (V_{perit}^C w_C), & \text{if } T_i > 0, \end{cases} \quad (S3.4)$$

where  $R_i$  is the rate (in  $\mu\text{g}$  per day) at which carboplatin is being administered and  $w_C$  is its molecular weight. When carboplatin is administered as a series of periodic boluses, with period of therapy  $\tau_C$  days, equation (S3.1) can be solved explicitly to give (cf. Equation (S2.9)):

$$C_{perit}(t) = C_{perit}(t=0) e^{-\mu_C \text{rem}(t, \tau_C)}, \quad (S3.5)$$

where  $C_{perit}(t=0)$  is the concentration of carboplatin in the intraperitoneal cavity immediately following an injection. When carboplatin is administered periodically as a continuous infusion, with each infusion

lasting  $T_i$  days and the period of therapy  $\tau_C$  days, equation (S3.1) can be solved explicitly to give:

$$C_{perit}(t) = \begin{cases} \frac{K_0}{\mu_C} \left(1 - e^{-\mu_C rem(t, \tau_C)}\right), & \text{if } rem(t, \tau_C) \leq T_i \\ \frac{K_0}{\mu_C} \left(e^{\mu_C rem(T_i, \tau_C)} - 1\right) e^{-\mu_C rem(t, \tau_C)}, & \text{if } rem(t, \tau_C) > T_i \end{cases}. \quad (\text{S3.6})$$

In the above discussion,  $T_i < \tau_C$ . Given its rapid rate of clearance from mouse plasma [6], we have also assumed that the intraperitoneal concentration of carboplatin at the end of each cycle of therapy is  $\sim 0$ . Thus, the complete system of equations governing the pharmacokinetics of carboplatin is given by equations (S3.2)- (S3.6).

We remark that if the amount of carboplatin to be administered in each round of therapy is fixed at  $D_C$   $\mu\text{g}$ , the initial concentration of carboplatin in the intraperitoneal cavity immediately following a bolus dose is  $C_{perit}(t=0) = \frac{D_C}{V_{perit}^C w_C}$   $\mu\text{M}$ , while in the case of continuous infusion, the rates of infusion are given by  $K_0 = \frac{D_C}{V_{perit}^C w_C T_i}$   $\mu\text{M}$  per day and  $R_i = \frac{D_C}{T_i}$   $\mu\text{g}$  per day.

### S3.2 Parameter Estimation

A list of parameter values with sources is provided in Table S3. For clarity, we discuss the estimation of those parameters values which could not be determined directly from the literature. The volume of distribution of carboplatin in the peritoneal cavity  $V_{perit}^C$  is taken to be the average of its volumes of distribution in the systemic circulation and peripheral tissue compartments. The rate of carboplatin extravasation from the peritoneal cavity into systemic circulation ( $\mu_C$ ) is taken to be the average of the rates of entry of carboplatin from the systemic circulation into the intracellular compartment and vice versa ( $K_{PT}^C$  and  $K_{TP}^C$  respectively).

In Witham et al. [1], a bolus dose of 30 mg/kg (equivalent to a dose  $D_C = 600$   $\mu\text{g}$  assuming a typical mouse weighs 200 g) was administered weekly to mice: we simulate equations (S3.2)- (S3.5) to generate similar plasma and tissue carboplatin concentration time-courses, using the equivalent dose  $D_C = 600$   $\mu\text{g}$ . The results plotted in Figure S2B reveal that plasma (black curve) and tissue (red curve) carboplatin

is cleared within 2-3 hours, and while the maximum plasma concentration  $C_{P_{max}}^b = 283.0 \mu\text{M}$ , the maximum tissue concentration is  $C_{T_{max}}^b = 131.1 \mu\text{M}$ . To illustrate the altered dynamics of carboplatin when it is administered via continuous infusion, we also simulate equations (S3.2) (S3.4) and (S3.6) for the same total dose  $D_C$ , and for an infusion time  $T_i = 12$  hours. The results plotted in Figure S2C reveal that plasma (black curve) and tissue (red curve) carboplatin reach steady states of  $14.3 \mu\text{M}$  and  $9.0 \mu\text{M}$ , respectively within 3 hours of therapy application and are rapidly cleared at the end of the infusion.

## S4 Simulation Methodology

The system of time-delayed ordinary, partial differential and algebraic equations used to simulate the treatment with carboplatin and ABT-737 of a growing tumor xenograft (equations (S1.1)-(S1.3), (S1.14)-(S1.18), (S2.25)-(S2.29) and (S3.2)-(S3.6)) is solved as follows. Due to their stiff nature, the drug pharmacokinetic and pharmacodynamic equations (S2.25)-(S2.29) and (S3.2)-(S3.6) are solved in the computing software Matlab using 'ode23s', an in-built solver for stiff equations. The following solution to the hyperbolic equation governing the evolution of arrested cells (S1.2) is constructed using the method of characteristics [7]:

$$M(t, a) = \alpha_C(C_T(t - a)) N(t - a) e^{-C_T(t-a) \int_{t-(a-a_{char})}^t (\rho_C + \rho_S r_X(X(u) - X_{phys})) du}, \quad t \geq a \quad (\text{S4.1})$$

The above equation and the solutions to the drug equations inform equation (S1.1), which governs the dynamics of proliferating cells. The fourth order explicit Runge-Kutta method is used to solve this equation.

Typical simulation results are presented in Figure S. They show the response of a tumor xenograft to weekly boluses of 30 mg/kg carboplatin treatment starting on day 19, as in [1]. The periodic therapy induces oscillations in tumor size, and hence cell numbers. Averaging cell numbers over the period of carboplatin administration (black curve in Figure S3) facilitates quantitative comparisons between tumor responses to the various treatment strategies that are discussed in the manuscript.

## S5 Parameter Estimation for Monoclonal Tumor Xenograft Growth

### Treatment

Where possible, the values of parameters relating to the growth rate of the tumor xenograft and its response to treatment are based on data from the literature. In cases where no data is available, parameter values were obtained by fitting (in a least squares sense) time-courses of cell numbers to data from [1] wherein IGROV-1 xenografts established in mice were left untreated (control) or treated periodically with a fixed dose of carboplatin or ABT-737 (or both) for 4 weeks. Briefly, the model was reduced to represent the different *in vivo* experimental systems: no therapy (control), ABT-737-only therapy, carboplatin-only therapy, and combined therapies involving carboplatin and ABT-737. The fits were carried out using the computing software Matlab's in-built nonlinear, curve-fitting tool, "lsqcurvefit". Care was taken to fit no more than 2-3 parameters to any given set of experimental data. Biologically realistic values were chosen for parameters for which no experimental data was available. The model equations for each case and the parameters being fit are reported below.

#### S5.1 No Therapy (Control) and ABT-737-only Therapy

The basic proliferation rate of IGROV-1 cells ( $\lambda_N$ ), the carrying capacity of their microenvironment ( $K$ ) and the Bax-dependent death rate of proliferating cells ( $r_X$ ) are fixed by simultaneously fitting time-courses of simulated cell numbers to tumor xenograft growth data taken from [1], wherein IGROV-1 xenografts established in mice were left untreated (control) or treated daily with a fixed dose (100 mg/kg) of ABT-737 administered intraperitoneally for 4 weeks, and tumor size recorded at regular intervals. The following equations for xenograft growth and treatment with ABT-737 are obtained from the full model system by setting the carboplatin concentrations  $C_{perit} = C_P = C_T = 0$ .

$$\frac{dN}{dt} = \lambda_N N \left(1 - \frac{N}{K}\right) - r_X X N, \quad (\text{S5.1})$$

$$A_{perit}(t) = \alpha_{perit}^* e^{-\mu_A rem(t, \tau_A)}, \quad (\text{S5.2})$$

$$\frac{dA_P}{dt} = \mu_A A_{perit} - K_A A_P, \quad (\text{S5.3})$$

$$B(A_C) = \frac{-(\zeta_1 \beta A_C + \zeta_2 \alpha_C \beta) + \zeta_1 \beta \sqrt{A_C^2 + \rho_1 \alpha_C A_C + \rho_2 \alpha_C^2}}{\bar{\nu}_1 A_C + \alpha_C \bar{\nu}_2}, \quad (\text{S5.4})$$

$$X(A_C) = -(\chi \sigma_1 A_C + \chi \alpha_C \sigma_2) + \chi \sigma_1 \sqrt{A_C^2 + \rho_1 \alpha_C A_C + \rho_2 \alpha_C^2}, \quad (\text{S5.5})$$

$$\frac{dA_C}{dt} = (K_{PC}^A A_P - K_{CP}^A A_C) \frac{\alpha_P}{\alpha_P - \alpha_C (dB/dA_C) + \alpha_P (dX/dA_C)}, \quad (\text{S5.6})$$

where

$$\alpha_{perit}^* = \begin{cases} 0, & \text{no therapy,} \\ \alpha_{perit}, & \text{ABT-737 therapy.} \end{cases} \quad (\text{S5.7})$$

The fits that minimize in a least squares sense the residual between simulated and experimental data are presented in Figure 1C of the main text. The values of  $\lambda_N$ ,  $K$  and  $r_X$  thus obtained are reported in Table S4.

## S5.2 Carboplatin-only and Carboplatin + ABT-737 Combination Therapy

Next, the maximal rate of proliferating cell become growth arrested in response to carboplatin ( $r_C$ ), the carboplatin-dependent rate at which arrested cells die ( $\rho_C$ ) and the sensitivity of the arrested cells to changes in Bax ( $\rho_S$ ) are fixed by simultaneously fitting simulated time-courses of cell numbers to tumor xenograft growth inhibition data taken from [1], wherein IGROV-1 xenografts established in mice were treated weekly with a fixed bolus dose (30 mg/kg) of carboplatin alone or in combination with a fixed daily dose (100 mg/kg) of ABT-737 administered intraperitoneally for 4 weeks, and tumor size recorded at regular intervals. The equations for xenograft treatment with carboplatin alone or in combination

with ABT-737 are:

$$\frac{dN}{dt} = \lambda_N N \left( 1 - \frac{N + \int_{t-a_r}^t M(t, a) da}{K} \right) - r_X X N - \alpha_C(C_T) N + M(t, a = a_r), \quad (\text{S5.8})$$

$$\frac{\partial M}{\partial t} + \frac{\partial M}{\partial a} = -(\rho_C + \rho_S r_X (X - X_{phys})) C_T(t - a) H(a - a_{char}) M, \quad (\text{S5.9})$$

$$A_{perit}(t) = \alpha_{perit}^* e^{-\mu_A rem(t, \tau_A)}, \quad (\text{S5.10})$$

$$\frac{dA_P}{dt} = \mu_A A_{perit} - \lambda_A A_P, \quad (\text{S5.11})$$

$$B(A_C) = \frac{-(\zeta_1 \beta A_C + \zeta_2 \alpha_C \beta) + \zeta_1 \beta \sqrt{A_C^2 + \rho_1 \alpha_C A_C + \rho_2 \alpha_C^2}}{\bar{\nu}_1 A_C + \alpha_C \bar{\nu}_2}, \quad (\text{S5.12})$$

$$X(A_C) = -(\chi \sigma_1 A_C + \chi \alpha_C \sigma_2) + \chi \sigma_1 \sqrt{A_C^2 + \rho_1 \alpha_C A_C + \rho_2 \alpha_C^2}, \quad (\text{S5.13})$$

$$\frac{dA_C}{dt} = (K_{PT}^A A_P - K_{TP}^A A_C) \frac{\alpha_P}{\alpha_P - \alpha_C (dB/dA_C) + \alpha_P (dX/dA_C)}, \quad (\text{S5.14})$$

$$C_{perit}(t) = C_{perit}(t=0) e^{-\mu_C rem(t, \tau_C)}, \quad (\text{S5.15})$$

$$\frac{dC_P}{dt} = \mu_C \frac{V_{perit}^C}{V_P^C} C_{perit} - K_C C_P - K_{PT}^C C_P + K_{TP}^C \frac{V_T^C}{V_P^C} C_T, \quad (\text{S5.16})$$

$$\frac{dC_T}{dt} = K_{PT}^C \frac{V_P^C}{V_T^C} C_P - K_{TP}^C C_T, \quad (\text{S5.17})$$

where

$$\alpha_C(C_T) = r_C \frac{C_T^2}{C_T^2 + K_{carb}^2}, \quad (\text{S5.18})$$

$$M(t, 0) = \alpha_C(C_T) N, \quad (\text{S5.19})$$

$$\alpha_{perit}^* = \begin{cases} 0, & \text{carboplatin-only therapy,} \\ \alpha_{perit}, & \text{combination therapy,} \end{cases} \quad (\text{S5.20})$$

and where  $X_{phys} = 27.83$  nM is the intracellular concentration of free Bax in the absence of ABT-737 therapy (see section S3.2 above). The fits that minimize in a least squares sense the residual between simulated and experimental data are presented in Figure 1D of the main text. The values of  $r_C$ ,  $\rho_C$  and  $\rho_S$  thus obtained are reported in Table S4.

### S5.3 Parameter Sensitivity

A sensitivity analysis was carried out by varying the parameters associated with the cellular response to carboplatin and ABT-737 that were previously estimated from experimental data. These include: the rate at which proliferating cells die ( $r_X$ , see equation (S1.14)); the concentration of carboplatin at which the rate of proliferating cell arrest is half its maximum value ( $K_{carb}$ ) and the maximum rate at which proliferating cells become growth arrested in response to carboplatin ( $r_C$ , see equation (S1.15)); and the rate at which arrested cells die in response to carboplatin-induced DNA damage ( $\rho_C$ ) and the sensitivity of arrested cells to intracellular Bax ( $\rho_S$ , see equation (S1.16)). In each case, the residual between simulated and experimental data is computed as each parameter is varied from its baseline estimate, and the resulting percentage increase in this residual is plotted as a function of the change in the value of parameter being varied.

Figures S4A,B reveal that the model predictions of tumor cell numbers are highly sensitive to  $r_X$  and  $\alpha_C$ . A 10% change over the baseline value of  $r_X$  increases the residual in the fits shown in Figure 1C by over 20% (Figure S4A), while a 14% change in  $\alpha_C$  has the same effect on the residual in these fits (Figure S4B). From Figure S4D, we observe that sensitivity to changes in  $\rho_C$  is less marked, with a 20% change in  $\rho_C$  over its baseline value predicted to result in a 20% increase in the residual of the fits shown in Figure 1D. The model is more robust to changes in  $K_{carb}$ : Figure S4C reveals that a change in  $K_{carb}$

of at least 50% over its baseline value is required to induce a 20% increase in the residual in the fits shown in Figure 1D. Model predictions are also robust to changes in  $\rho_S$  (see Figure S4E). However, for very small values of  $\rho_S$ , the residual in the fits shown in Figure 1D increases rapidly.

Finally, we investigate the effect of varying the carboplatin infusion time  $T_i$  on tumor xenograft size at the end of 4 weeks of treatment with carboplatin alone, fixing its weekly dose at 30 mg/kg, as in [1]. Figure S4F shows how the numbers of proliferating and arrested cells averaged over the period of carboplatin administration change as  $T_i$  is varied from 0 (bolus) to 5 days. An infusion time of between 1 and 2 hours is predicted to maximize tumor growth inhibition. Increasing  $T_i$  above 2 hours results in a rapid decrease in the level of tumor growth inhibition, with infusions lasting 2 or more days having almost no effect on final xenograft sizes. This is because slow infusions of carboplatin lead to low tissue concentrations of the drug, so that the level of DNA damage induced in proliferating cells is minimal. Interestingly, infusions lasting 8 hours are predicted to give the highest fraction of cells in a growth arrested state. This is possibly due to a high rate of proliferating cell arrest coupled with a relatively low rate of arrested cell death. We remark that since arrested cells have previously been shown to be highly sensitive to intracellular Bcl-xL levels [8], when carboplatin is given with ABT-737, a carboplatin infusion time of 8 hours is expected maximally to exploit the synergy between the two drugs. Figures 3, 4 and 5 of the main text corroborate this prediction.

From the above discussion, we expect that the optimal protocols predicted by our model will be relatively robust to changes in the parameters  $\rho_C$ ,  $K_{carb}$  and  $\rho_S$  and highly sensitive to variations in  $r_X$ ,  $\alpha_C$  or  $T_i$ .



## References

- [1] Witham J, Valenti MR, De-Haven-Brandon AK, et al. The Bcl-2/Bcl-xL family inhibitor ABT-737 sensitizes ovarian cancer cells to carboplatin. *Clin Cancer Res* 2007;13:7191-8.
- [2] Bajaj G, Yeo Y. Drug delivery systems for intraperitoneal therapy. *Pharm Res* 2010;27:735-738.
- [3] Lukas G, Brindle SD, Greengard P. The route of absorption of intraperitoneally administered compounds. *J Pharmacol Exp Ther* 1971;178:562-564.
- [4] Chen C, Cui J, Zhang W, Shen P. Robustness analysis identifies the plausible model of the Bcl-2 apoptotic switch. *FEBS Lett* 2007;581:5143-5150.
- [5] Hua F, Cornejo MG, Cardone MH, Stokes CL, Lauffenburger DA. Effects of Bcl-2 levels on Fas signaling-induced caspase-3 activation: molecular genetic tests of computational model predictions. *J Immunol* 2005;175:985-995.
- [6] Siddik ZH, Newell DR, Boxall FE, Harrap KR. The comparative pharmacokinetics of carboplatin and cisplatin in mice and rats. *Biochem Pharmacol* 1987;36:1925-32.
- [7] Jain HV, Byrne HM. Qualitative analysis of an integro-differential equation model of periodic chemotherapy. *Appl Math Lett* 2012;25:2132-6.
- [8] Jain HV, Meyer-Hermann M. The molecular basis of synergism between carboplatin and ABT-737 therapy targeting ovarian carcinomas. *Cancer Res* 2011;71:705-15.

## Figure Legends

**Figure 1:** ABT-737 pharmacokinetics in a mouse. **A**, ABT-737 is periodically administered intraperitoneally (i.p.), into the peritoneal cavity from where it enters the systemic circulation. From here, ABT-737 enters the intracellular compartment, and is also cleared from the body. Figures showing **B**, intraperitoneal, **C**, plasma and **D**, intracellular ABT-737 concentration time-courses when 100 mg/kg of the drug is administered daily starting on day 5. **E**, Resultant intracellular Bcl-xL (black curve) and Bax (red curve) concentration time-courses.

**Figure 2:** Carboplatin pharmacokinetics in a mouse. **A**, Carboplatin is periodically administered intraperitoneally (i.p.), into the peritoneal cavity from where it enters the systemic circulation. From here, carboplatin is distributed to peripheral organs and tissues with poor vascular perfusion, and is also cleared from the body. Figures showing plasma (black curve) and peripheral tissue (red curve) carboplatin concentration time-courses corresponding to a dose of 30 mg/kg, given **B**, as a bolus, or **C**, as a continuous infusion lasting 12 hours.

**Figure 3:** Tumor xenograft response to 30 mg/kg of carboplatin-only therapy administered as a bolus dose every 7 days, starting on day 19 (black arrow) is simulated. Figure shows total cell number (red curve) and total cell number averaged over the period of therapy administration (black curve) versus time.

**Figure 4: A-E**, Model sensitivity to key parameters. Variation of the parameters from their baseline values is plotted on the x-axis. The % change in the Euclidean norm of the error over its value from performing fits of the model to experimental data (see Figures 1B,C in main manuscript) is plotted on the y-axis. **F**, Predicted average total (black curve), proliferating (red curve) and growth arrested (blue curve) tumor cell numbers at the end of 4 weeks of treatment of a tumor xenograft with 30 mg/kg carboplatin administered weekly, as the time of infusion of each dose is varied.

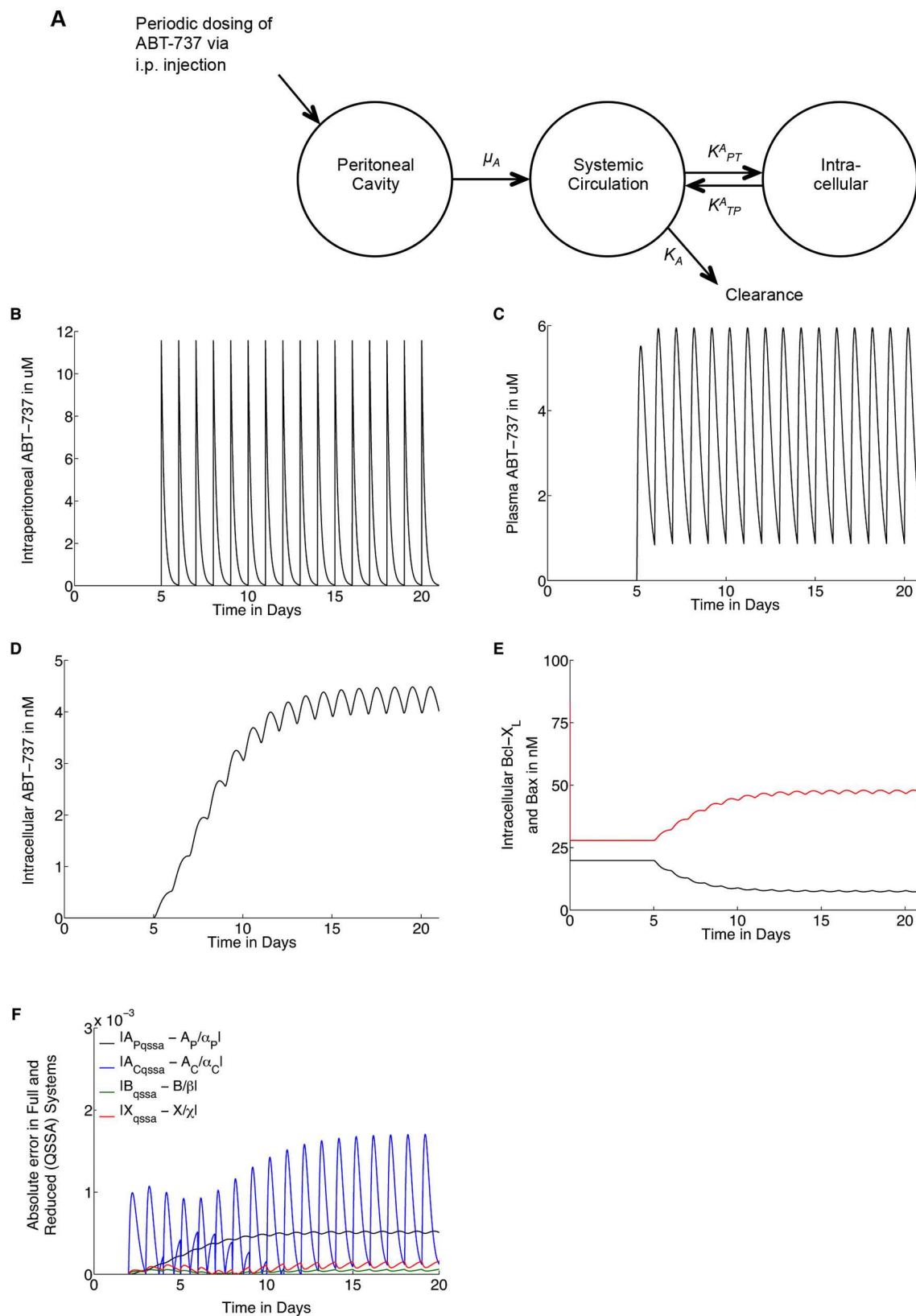


Figure 1: ABT pharmacokinetics

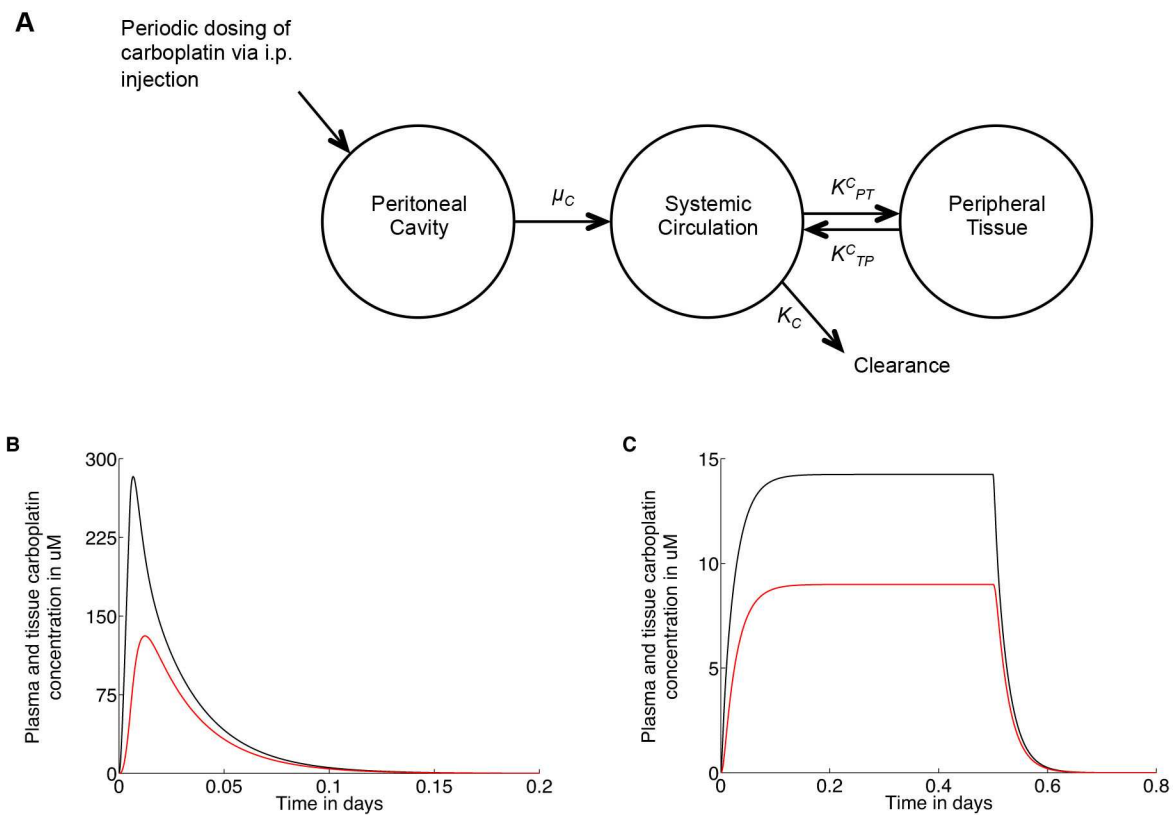


Figure 2: Carboplatin pharmacokinetics

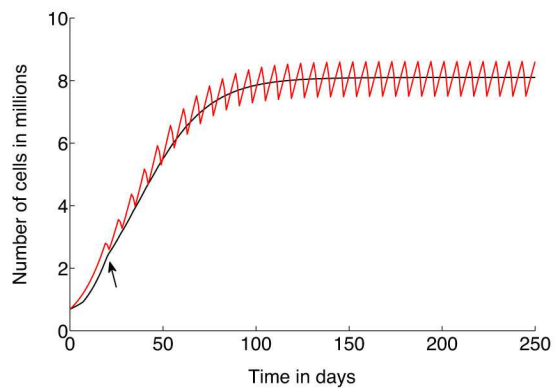


Figure 3: Typical Simulation Result

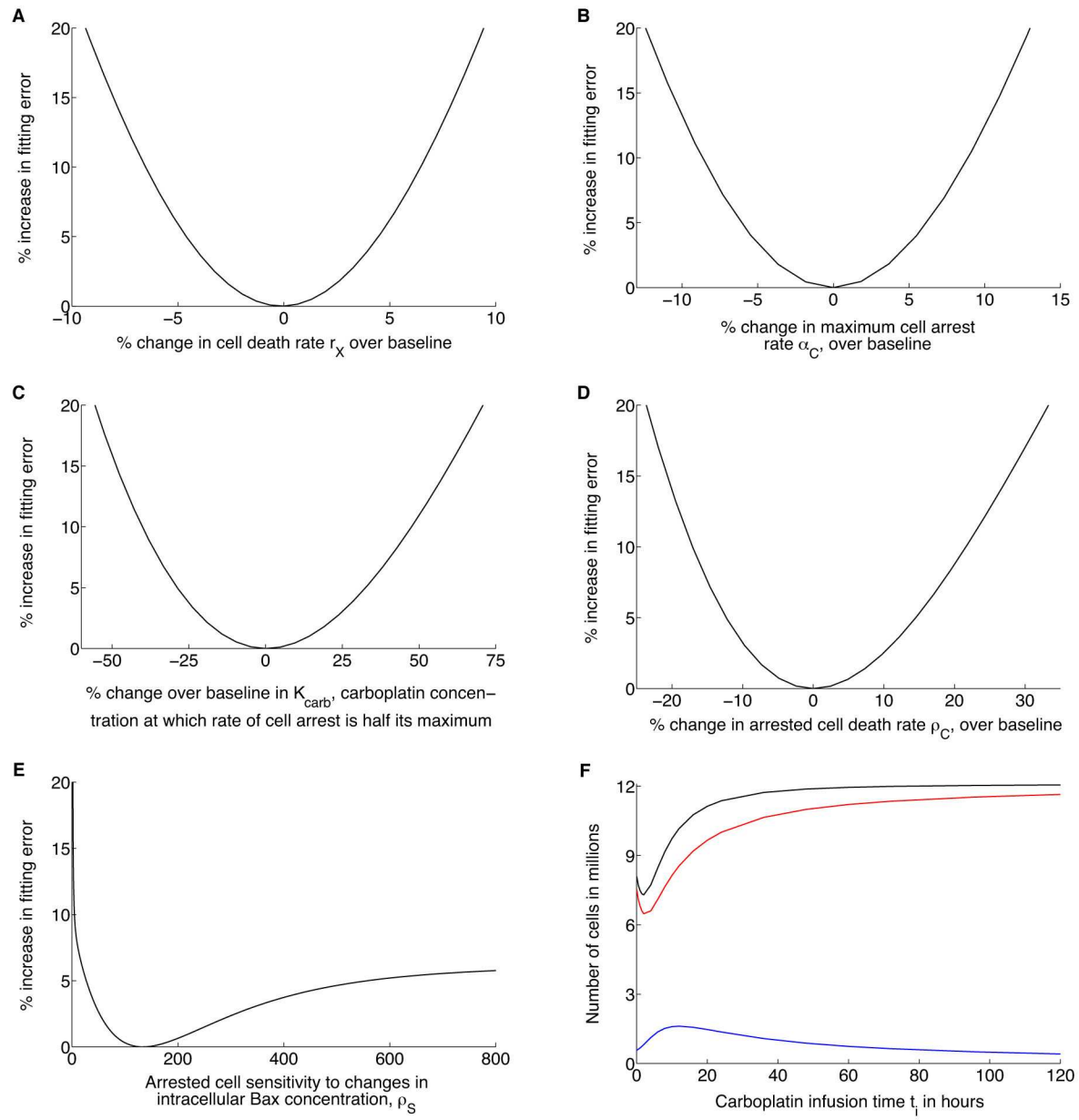


Figure 4: Parameter Sensitivity

Table S1: List of parameter values relating to ABT-737 pharmacokinetics and pharmacodynamics.

Parameter	Value	Source
$\tau_A$	1 day	[1]
$\alpha_{perit}$	$11.56 \times 10^3$ nM	[2]
$\mu_A$	6 per day	see text
$\lambda_A$	3.37 per day	[2]
$K_{CP}^A$	2.40 per day	see text
$K_{PC}^A$	$3 \times 10^{-3}$ per day	see text
$K_A$	3.36 per day	see text
$k_a^A$	172.80 per day per nM	[3,4] <sup>1</sup>
$k_d^A$	172.80 per day	[4] <sup>2</sup>
$k_a^X$	172.80 per day per nM	[3]
$k_d^X$	1728 per day	[3]
$\beta$	75 nM	[3]
$\chi$	83.33 nM	[3]

## References

- [1] Witham J, Valenti MR, De-Haven-Brandon AK, et al. The Bcl-2/Bcl-xL family inhibitor ABT-737 sensitizes ovarian cancer cells to carboplatin. Clin Cancer Res 2007;13:7191-8.
- [2] Tse C, Shoemaker AR, Adickes J et al. ABT-263: a potent and orally bioavailable Bcl-2 family inhibitor. Cancer Res 2008;68:3421-3428.
- [3] Hua F, Cornejo MG, Cardone MH, Stokes CL, Lauffenburger DA. Effects of Bcl-2 levels on Fas signaling-induced caspase-3 activation: molecular genetic tests of computational model predictions. J Immunol 2005;175:985-95.
- [4] Oltersdorf T, Elmore SW, Shoemaker AR, et al. An inhibitor of Bcl-2 family proteins induces regression of solid tumours. Nature 2005;435:677-81.

<sup>1</sup>It is assumed that rate of the forward reaction of ABT-737 with Bcl-2/xL is similar to that of Bax binding to Bcl-2.

<sup>2</sup>The dissociation constant for ABT-737 binding Bcl-2/xL is  $\sim 1$  nM.

Table S2: List of non-dimensional parameter values relating to ABT-737 pharmacokinetics and pharmacodynamics.

Parameter	Expression	Value
$\bar{\mu}_A$	$\tau_A \mu_A$	6
$\bar{\eta}_A$	$\mu_A \tau_A \alpha_{perit} / \alpha_P$	11.66
$\bar{K}_A$	$K_A \tau_A$	3.36
$\epsilon$	$1 / (k_d^X \tau_A)$	$5.79 \times 10^{-4}$
$\bar{\kappa}_0$	$k_d^X \tau_A \alpha_C / \alpha_P$	1.30
$\bar{\kappa}_1$	$K_{PC}^A \tau_A \alpha_P / \alpha_C$	3.96
$\bar{\kappa}_2$	$K_{CP}^A \tau_A$	2.40
$\bar{\gamma}_1$	$\beta / \alpha_C$	16.70
$\bar{\gamma}_2$	$\beta / \chi$	0.90
$\bar{\nu}_1$	$k_a^A \alpha_T / k_d^X$	0.45
$\bar{\nu}_2$	$k_d^A / k_d^X$	0.10
$\bar{\nu}_3$	$k_a^X \chi / k_d^X$	8.33
$\zeta_1$	$\bar{\nu}_1 / (2\bar{\gamma}_2\bar{\nu}_3)$	0.03
$\zeta_2$	$\bar{\nu}_2(1 + \bar{\nu}_3 - \bar{\nu}_3\bar{\gamma}_2) / (2\bar{\gamma}_2\bar{\nu}_3)$	0.01
$\sigma_1$	$\bar{\nu}_1 / (2\bar{\nu}_2\bar{\nu}_3)$	0.27
$\sigma_2$	$(1 - \bar{\nu}_3 + \bar{\nu}_3\bar{\gamma}_2) / (2\bar{\nu}_3)$	0.01
$\rho_1$	$2\bar{\nu}_2(1 + \bar{\nu}_3 + \bar{\nu}_3\bar{\gamma}_2) / \bar{\nu}_1$	7.50
$\rho_2$	$\bar{\nu}_2^2 [1 + 2\bar{\nu}_3(1 + \bar{\gamma}_2) + \bar{\nu}_3^2(1 - \bar{\gamma}_2)^2] / \bar{\nu}_1^2$	1.65



Table S3: List of parameter values relating to carboplatin pharmacokinetics.

Parameter	Value	Source
$w_C$	371.25 Da	pubchem database
$\mu_C$	201.60 per day	see text
$K_{PT}^C$	201.60 per day	[1]
$K_{TP}^C$	201.60 per day	[1]
$K_C$	90.72 per day	[1]
$V_{perit}^C$	$2.50 \times 10^{-3}$ L	see text
$V_P^C$	$2.50 \times 10^{-3}$ L	[1]
$V_T^C$	$3.96 \times 10^{-3}$ L	[1]

#### References

- [1] Siddik ZH, Newell DR, Boxall FE, Harrap KR. The comparative pharmacokinetics of carboplatin and cisplatin in mice and rats. *Biochem Pharmacol* 1987;36:1925-32.

Table S4: List of parameter values relating to xenograft growth and treatment.

Parameter	Value	Source
$\lambda_N$	0.13 per day	[1]
$\lambda_R$	0.13 per day	<sup>1</sup>
$K$	18.18 cells (in millions)	[1]
$r_X$	$1.53 \times 10^{-3}$ per nM Bax per day	[1]
$r_C$	5.47 per day	[1]
$K_{carb}$	21 $\mu$ M	[2]
$\rho_C$	$8.21 \times 10^{-3}$ per $\mu$ M carboplatin per day	[1]
$\rho_S$	134 per $\mu$ M carboplatin	[1]
$\alpha_{perit}$ (corresponding to 100 mg/kg ABT-737)	11.56 $\mu$ M	[1]
$\kappa_{perit}$ (corresponding to 30 mg/kg carboplatin)	500.36 $\mu$ M	[1]
$X_{phys}$	27.83 nM	[3]

#### References

- [1] Witham J, Valenti MR, De-Haven-Brandon AK, et al. The Bcl-2/Bcl-xL family inhibitor ABT-737 sensitizes ovarian cancer cells to carboplatin. Clin Cancer Res 2007;13:7191-8.
- [2] Jain HV, Meyer-Hermann M. The molecular basis of synergism between carboplatin and ABT-737 therapy targeting ovarian carcinomas. Cancer Res 2011;71:705-15.
- [3] Hua F, Cornejo MG, Cardone MH, Stokes CL, Lauffenburger DA. Effects of Bcl-2 levels on Fas signaling-induced caspase-3 activation: molecular genetic tests of computational model predictions. J Immunol 2005;175:985-95.



## RECENT REPORTS

12/88	The kinetics of surfactant desorption at the airsolution interface	Morgan Breward Griffiths Howell Penfold Thomas Tucker Petkov Webster
12/89	An experimental and theoretical investigation of particlewall impacts in a T-junction	Vigolo Griffiths Radl Stone
12/90	Transitions through Critical Temperatures in Nematic Liquid Crystals	Majumdar Ockendon Howell Surovyatkina
12/91	Biaxial defect cores in nematic equilibria: an asymptotic result	Majumdar Pisante Henao
12/92	The Three Sphere Swimmer in a Nonlinear Viscoelastic Medium	Curtis Gaffney
12/93	Diffusion of multiple species with excluded-volume effects	Bruna Chapman
12/94	The Mechanics of a Chain or Ring of Spherical Magnets	Hall Vella Goriely
12/95	On-Lattice Agent-based Simulation of Populations of Cells within the Open-Source Chaste Framework	Figueredo Joshi Osborne Byrne Owen
12/96	Mathematical Biomedicine and Modeling Avascular Tumor Growth	Byrne
12/97	Inference of the genetic network regulating lateral root initiation in Arabidopsis thaliana	Muraro Voß Wilson Bennett Byrne De Smet Hodgman King
12/98	Axisymmetric bifurcations of thick spherical shells under inflation and compression	deBotton Bustamante Dorfmann
12/99	Calculus from the past: Multiple Delay Systems arising in Cancer Cell Modelling	Wake Byrne

12/103	Control and optimization of solute transport in a porous tube	Griffiths Howell Shipley
12/104	Air-cushioning in impact problems	Moore Ockendon Oliver
12/105	Strain controlled biaxial stretch: An experimental characterization of natural rubber	Pancheri Dorfmann
12/106	Non-linear modeling of active biohybrid materials	Paetsch Dorfmann
12/107	Coalescence of Liquid Drops: Different Models Versus Experiment	Sprittles Shikhmurzaev
12/108	Adjoint Based A Posteriori Analysis of Multiscale Mortar Discretizations with Multinumerics	Tavener Willey
12/109	Dynamics of mechanically induced fiber reorientation in the material reinforced by two families of fibers	Melnik Goriely
12/110	Multiscale stochastic reaction-diffusion modelling: application to actin dynamics in filopodia	Erban Flegg Papoian

**Copies of these, and any other OCCAM reports can be obtained from:**

**Oxford Centre for Collaborative Applied Mathematics  
Mathematical Institute  
24 - 29 St Giles'  
Oxford  
OX1 3LB  
England  
[www.maths.ox.ac.uk/occam](http://www.maths.ox.ac.uk/occam)**